A Novel Approach to Micro-Telemanipulation with Soft Slave Robots: Integrated Design of a Non-overshooting Series Elastic Actuator

by

Ozan Tokatlı

Submitted to the Graduate School of Sabancı University
in partial fulfillment of the requirements for the degree of
Master of Science

Sabancı University

August, 2010

A Novel Approach to Micro-Telemanipulation with Soft Slave
Robots: Integrated Design of a Non-overshooting Series Elastic
Actuator

APPROVED BY:

Assist. Prof. Dr. Volkan Patoğlu
(Thesis Advisor)   ....

Prof. Dr. Asif Sabanovic   ....
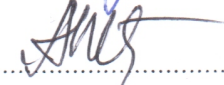
Assoc. Prof. Dr. Kemalettin Erbatur ....

Assist. Prof. Dr. Kürşat Şendur   ....

Assoc. Prof. Dr. Erhan Budak   ....

DATE OF APPROVAL: 05.08.2010

A Novel Approach to Micro-Telemanipulation with Soft Slave Robots: Integrated Design of a Non-overshooting Series Elastic Actuator

Ozan Tokatlı

ME, Master of Science, 2010

Thesis Supervisor: Assist. Prof. Dr. Volkan Patoğlu

Abstract

Micro mechanical devices are becoming ubiquitous as they find increasing uses in applications such as micro-fabrication, micro-surgery and micro-probing. Use of micro-electromechanical systems not only offer compactness and precision, but also increases the efficiency of processes. Whenever mechanical devices are used to interact with the environment, accurate control of the forces arising at the interaction surfaces arise as an important challenge.

In this work, we propose using a series elastic actuation (SEA) for micromanipulation. Since an SEA is an integrated mechatronic device, the mechanical design and controller synthesis are handled in parallel to achieve the best overall performance.

The mechanical design of the μSEA is handled in two steps: type selection and dimensional synthesis. In the type selection step, a compliant, half pantograph mechanism is chosen as the underlying kinematic structure of the coupling element. For optimal dimensioning, the bandwidth of the system, the disturbance response and the force resolution are considered to achieve good control performance with high reliability. These objectives are achieved by optimizing the manipulability and the stiffness of the mechanism along with a robustness constraint.

In parallel with the mechanical design, a force controller is synthesized. The controller has a cascaded structure: an inner loop for position control and an outer loop for force control. Since excess force application can be

detrimental during manipulation of fragile objects; the position controller of the inner loop is designed to be a non-overshooting controller which guarantees the force response of the system always stay lower than the reference value.

This self-standing μSEA system is embedded into a 3-channel scaled teleoperation architecture so that an operator can perform micro-telemanipulation. Constant scaling between the master and the slave is implemented and the teleoperator controllers preserve the non-overshooting nature of the μSEA.

Finally, the designed μSEA based micro-telemanipulation system is implemented and characterized.

Yumuşak Esir Robotları Kullanılan Mikro-Telemanipülasyona Yeni Bir Yaklaşım: Tümleşik Seri Elastik Eyleyici Tasarımı

Ozan Tokatlı

ME, Yüksek Lisans Tezi, 2010

Tez Danışmanı: Yrd. Doç. Dr. Volkan Patoğlu

Anahtar Kelimeler: Gürbüz Eniyi Tasarım, Referansı Aşmayan Kuvvet Denetimi, Mikro Seri Elastik Eyleyici, Mikro Telemanipülasyon, Mikrosistemler

Özet

Mikro mekanik sistemler, mikro üretim, mikro cerrahi, mikro manipülasyon gibi uygulama alanlarında daha çok kullanılmaktadır. Mikro sistemler, kompaktlığı ve hassasiyeti arttırmakla kalmamakta, ayrıca uygulamaların verimini de geliştirmektedir. Eğer bahsedilen uygulamada, robot ve çevresinin fiziksel olarak ilişkiye girmesi söz konusu ise robotun sonlandırıcı uzayındaki kuvvetin hassas bir şekilde kontrol edilmesi gerekmektedir.

Bu çalışmada, seri elastik eyleyici kavramının (SEE) mikro manipülasyon için nasıl kullanılabileceği anlatılmaktadır. SEE'ler tümleşik bir mekatronik sistem olduğundan ötürü mekanik tasarım ve denetleyici sentezi paralel bir şekilde yürütülmelidir. Böylece SEE'den en iyi verim alınabilecektir.

μSEE'nin mekanik tasarımı iki aşamada yapılmıştır: tip seçimi ve boyutsal sentez. Tip seçiminde esnek bağlantılı, kinematik yetersiz, yarı-pantograf mekanizması μSEE'nin temel kinematik yapısı olarak seçilmiştir. Boyutsal sentez aşamasında, sistemin bant genişliği, dışarıdan gelen bozucu etkileri yadsıması ve kuvvet çözünürlüğü ele alınarak eniyi başarımı verecek gürbüz yapılanışlar aranmıştır. Bu istekler, sistemin gürbüzlüğünü de göz önüne alarak, sistemin idare edilebilirliği (manipulability) ve katılığı (stiffness) eniyilenilerek başarılmaya çalışılmıştır.

Mekanik tasarıma paralel olarak kuvvet denetleyicisi sentezlenmiştir. Bu kuvvet denetleyicisi kademeli bir yapıya sahiptir: iç döngüde bir pozisyon denetleyicisi, dış döngüde kuvvet denetleyici bulunmaktadır. Uygulamalar için robotun uygulayacağı fazladan kuvvet zararlı olabileceğinden ötürü referansı

aşmayan denetleyici tasarlanmıştır. Böylece her koşulda robotun kuvvet cevabı referansa eşit veya refesansın altında olmuştur.

Tümleşik tasarımı yapılan μSEE sistemi 3-kanallı teleoperaston mimarisine dahil edilmiştir. Böylece, bir operatör micro manipülasyon işlemleri gerçekleştirebilecektir. Efendi ve esir robotlar arasında sabit bir ölçeklendirme kullanılmıştır ve bu teleoperatör μSEE sisteminin referansı aşmama özelliğini korumaktadır.

Son olarak, tasarımı yapılan μSEE'ye dayanan mikro telemanipülasyon sistemi uygulanmış ve karakterizasyonu yapılmıştır.

Acknowledgements

It is a great pleasure to extend my gratitude to my thesis advisor Assist. Prof. Dr. Volkan Patoğlu for his precious guidance and support. I am greatly indebted to him for his supervision and excellent advises throughout my Master study. I would gratefully thank Prof. Dr. Asif Sabanovic, Assoc. Prof. Dr. Kemalettin Erbatur, Assist. Prof. Dr. Kürşat Şendur and Assoc. Prof. Dr. Erhan Budak for their feedbacks and spending their valuable time to serve as my jurors.

I would like to acknowledge the financial support provided by The Scientific & Technological Research Council of Turkey (TÜBİTAK) through my Master education under BİDEB scholarship.

Many thanks to my friends, Aykut Cihan Satıcı, Melda Ulusoy, Ahmetcan Erdoğan, Alper Ergin, Can Palaz, Kadir Haspalamutgil, Hakan Ertaş, Elif Hocaoğlu and Neşe Tüfekçiler for making the laboratory enjoyable and memorable.

Finally, I would like to thank my family for all their love and support throughout my life.

Contents

List of Figures

List of Tables

Chapter I

1 Introduction

Micro mechanical devices are becoming ubiquitous as they find increasing uses in applications such as micro-fabrication, micro-surgery and micro-probing. Use of micro-electromechanical systems not only offer compactness and precision, but also increases the efficiency of processes. Whenever mechanical devices are used to interact with the environment, accurate control of the forces arising at the interaction surfaces arise as an important challenge. The situation is not any different at the micro scale; therefore, force control in micro mechanisms is an integral part of the the robotics research in microsystems.

The aim of this thesis is to introduce a force controlled micro device that can be used in micro manipulation tasks. The proposed manipulator design is based on Series Elastic Actuation (SEA) which is an approach to force control. Although many devices operating in micro level have the ability to control the force at its en effector, their approach to force control is mostly rely on force sensor. On the other hand, a series elastic actuator utilizes a position sensor to achive accurate control of the force at its end effector. Due to its simplicity and robustness SEAs are practically used in robotic applications of macro level. The purpose of this thesis is to deliberately introduce the SEA approach to force controlled micro manipulation.

The rest of this chapter is organized as follows: the manipulation techniques in microsystem is introduced in 1.1. The commonly used force control methodologies in the literature is overviewed in 1.2. The series elastic actuation approach to force control is covered in 1.2.1 and finally, the contribution of this thesis is given in 1.3.

1.1 Manipulation in Microsystems

As the scale of the applications reduce in size, the accuracy and the physical limits of the problems change accordingly. However, the need for manipulating objects remain intact. Because of this manipulation needs micro manipulation is a fertile topic for robotics study. This section investigates some of the fundamental manipulation techniques used in microsystems but before searching for manipulators, it is better to get informed about the changes of the physics due to the change in the scale of the problem.

1.1.1 Effect of Scale Difference

As the scale of the problem decrease from macro to micro the governing forces acting in the system change. This is a change of becoming dominant or indistinguishable. The behavior of the forces due to scaling can be explained by the scaling laws and reader can refer to [1] for a nice overview of the results of scaling laws in different subjects.

As the scale of the problem decreases, the dynamic related forces, like Coriolis, become negligible. Hence, it can be stated that microsystems are pure kinematic structures. On the other hand, surface tension forces or adhesive forces become dominant in the system. These changes bring some interesting results that are not observable in macro systems. For instance,

although holding a micro sized object can be successfully attained, releasing it may not be possible due to the adhesive forces which bounds the object to the device's end effector. As a result, being aware of these changes, the design of such micro manipulators should be cautiously handled.

1.1.2 Micro Manipulation Techniques

Manipulation techniques in microsystems is not restricted with grippers. Many different techniques, which are mostly utilizing some interesting phenomenon, exist. Such techniques can be listed as micro probe, micro gripper, atomic force microscopy [2], optical tweezers [3, 4].

Grippers are also used in manipulation task in micro systems. Many gripper design is based on flexure joint (or compliant) mechanism. An example of flexure hinge based gripper design can be seen in [5]. In [6], a force controlled micro gripper which is combinin macro and micro actuation can be seen. This device is also a flexure hinged mechanism with multiple degrees of freedom is available for manipulation. Another micro-gripper example with an integrated force sensor can be seen in [7]. Xu and Zhu introduced an optimal micro gripper design with a force sensor mounted on the system. A strain gauge is used as the force sensor and the sensor arrangement that will minimize the adverse effects of vibration is searched. A micro assembly system using a micro gripper is introduced in [8]. The system consist of 4 different components one of which is a voice-coil driven flexure mechanism based micro gripper.

Another manipulation method used in microsystems is micro probe. In [9], a micro probe with 3 degrees of freedom is designed. This micro probe is mounted with piezoelectric actuators and sensors so that accurate motion

control is achieved. As an important aspect of the micro probe, 3 axes of the system can be measured accurately. Wenming and Hui presented a micro probe with a force sensing capability in [10]. This micro probe is used to manipulate cells. Another interesting work on micro probes is [11]. In this paper, a micro probe which operates in its axial direction is designed. A nonlinear geometry, which has a zig-zag shaped cross section, is designed for manipulation and it is argued that the vertical micro probe improves the quality of manipulation.

Another commonly used micro-manipulation technique is atomic force microscopy (AFM). An AFM device is a resonating beam which scans the surface of the object. The glare of the AFM is not just manipulating micro objects, it can be used to manipulate single atoms too. An example of cell manipulation with AFM can be seen in [12]. Another cell manipulation example is in [13]. In these works, the forces used to obtain image from the surface is increased so that living cells can be carried in the environment.

Optical tweezer are introduced to the literature in 1986. Since then, there has been an extensive research on the manipulation with optical tweezers. A neat investigation of optical tweezer technology can be found in [14]. An optical tweezer is a strongly focused beam of light is used to trap micro objects. Small objects, like 5nm, can be trapped in an optical tweezer and forces up to 100pN can be applied on the object. The most impressive aspect of the optical tweezers is their force resolution which is around 100aN. Basdogan *et al.* [15], utilized an optical tweezer in micro manipulation with haptic feedback. In [16], manipulation of cells using optical tweezers is investigated and verified with experiments.

1.2 Force Control Methodologies

Force control methods available in the literature can be grouped into two categories: direct and indirect approaches. In direct force control approach, force feedback loop is implemented in the system, on the other hand, in indirect method, force controlled is achieved through motion control. In [17], extensive overview of explicit force control strategies can be found. The explicit force control strategies can be based on force or position. Force based approach relies on force sensor information and PID controller is used in the control loop. Position based explicit force controller utilizes the cheap, robust positions sensors for obtaining accurate force control. This structure of controller has a cascaded form where a position controller is implemented in the inner loop and a force controller is in the outer loop. The analysis of Volpe and Khosla revealed that integral control is the best performing controller choice in explicit force control.

Another force control approach is impedance control [18]. The aim of the impedance control is to control the relation between the force and the velocity of the end effector. In an impedance controlled device, as the end effector is move, the reaction of the robot will preserve the force at the end effector according to the reference force signal. This method do not require force sensor but needs accurate model.

Admittance control is another force control method which is very similar to the impedance control except the fact that it is reciprocal of it. In admittance control, using a force sensor, the force signal is fed back to the controller and the robot reacts by changing it position. Using this control approach non-backdrivable devices can be turned into backdrivable manipulators.

A very nice review of force control for robotic manipulators can be found

in [19].

1.2.1 Series Elastic Actuation

Series elastic actuators (SEA) are introduced to the literature in the mid 90s. Since then they are increasingly used in both R&D and industrial applications. The logic behind an SEA is as simple as the Hooke's law for springs. Before delving into the idea of SEA, the basic structure of a force sensor worths to be explained.

As a common property, every material exhibit some amount of elastic deformation which is a deformation that can be recovered after the load on the system is removed. This behavior is very similar to the behavior of a helical spring which deflects up to a certain amount under loading and once the load is released the spring turns back to its initial configuration. This is the fundamental idea behind the force sensing devices. Those devices, whether it is a piezo resistive material, a strain gauge or a transducer, convert the displacement information into electric signal. From this point of view the working principle of a force sensor is companion to the working principle of a helical spring despite the fact that helical spring do not make a conversion from displacement to any other signal.

In a robotic system, where a force sensor is installed, the contact force between the robot end effector and the environment can be controlled using the force sensor information. However, there are certain drawbacks in using a force sensor. First of all, placing a force sensor at the end effector of the robot creates a non-collocation in the system which is illustrated in Figure 1.1. In the figure, the robotic manipulator is installed a force sensor which has its own dynamics. This new dynamics introduce significant poles and zeros.

Therefore, it can effect the stability of the robotic manipulator. Figure 1.2 depicts the root locus plot of a noncollocated robotic manipulator. Due to this non-collocation, the stability of the system can only be guaranteed for bounded closed loop feedback gains. In summary, using a force sensors places a upper bound on the gain of the system that can be used in feedback [20]. Another (minor) disadvantage is that a force sensor supplies a noisy signal to the system. This noise signal can be filtered out by signal processing however signal conditioning may not yield to a signal with enough smoothness. And also it should not be ignored that a signal conditioner is an extra cost to the user.
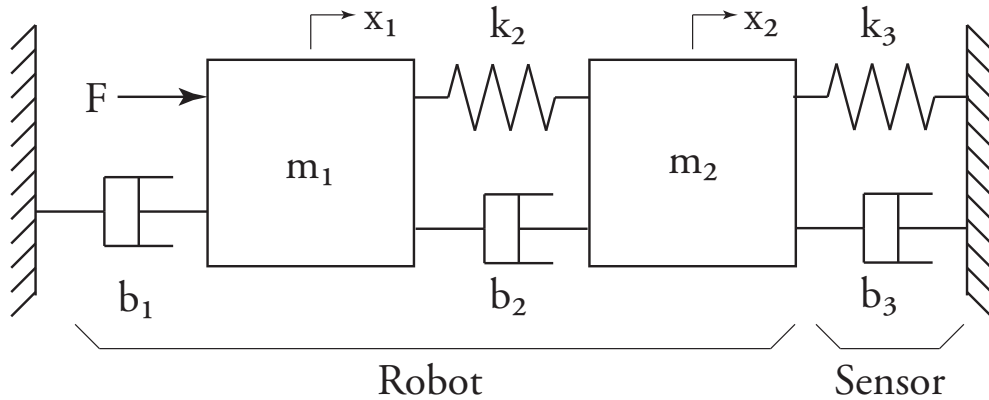
Figure 1.1: A robotic manipulator with a force sensor.

As it is explained in the previous paragraph, the force sensor is basically a spring which has a certain stiffness. This "spring" has a very high stiffness rate, for instance, ATI Nano17 transducer has a stiffness of $10^7 \ N/m$. Interpret this stiffness as proportional gain in the closed-loop system. As it is known that due to non-collocation there is an upper limit for the closed loop gains which is a combination of the stiffness of the transducer and the controller gain. For a high stiffness force sensor, low controller gains have to
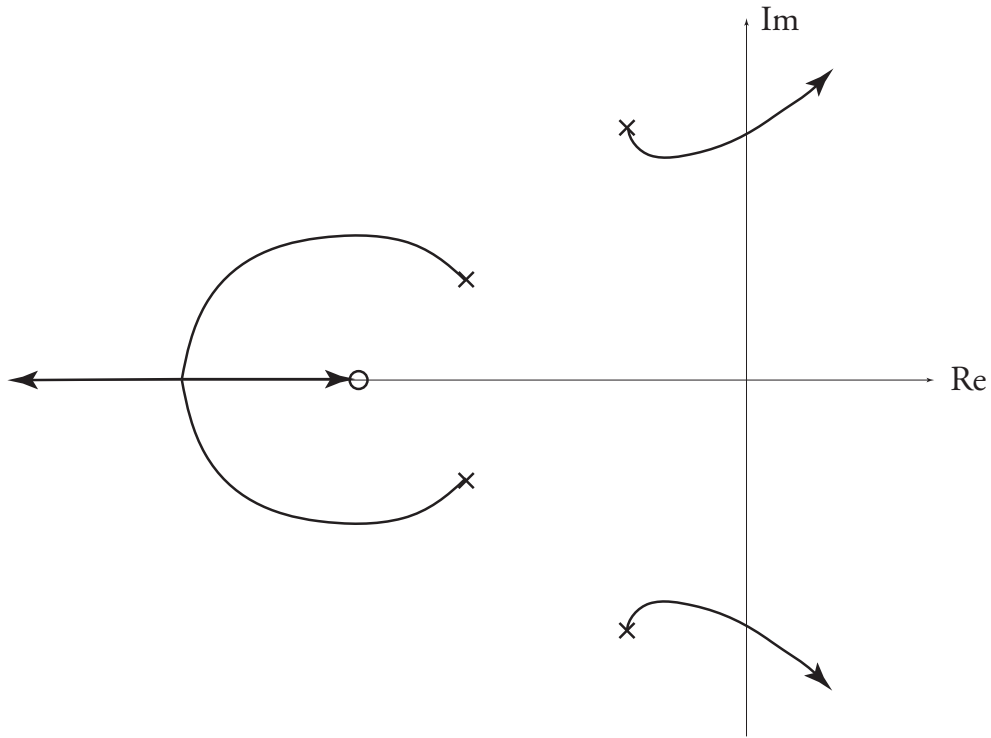
Figure 1.2: Root locus of the robotic manipulator with noncollocation.

be used in order to preserve the stability of the system. Hence only a slow controller can be implemented. The question to ask is whether the gain in the force sensor can be transfered to the controller so that a better controller can be implemented. The answer to this question is series elastic actuation.

Use of an SEA for force control at micro scale is advantageous, since it alleviates the need for high-precision force sensors/actuators and allows precise control of the force exerted by the actuator through typical position control of the deflection of the compliant coupling element. In particular, SEA introduces a compliant element between the actuator and the environment, then measures and controls the deflection of it. That is, an SEA transforms the force control problem into a position control problem [21] that can be

addressed using well established motion control strategies. Even though all force measurement techniques depend on measuring deflection of some compliant element by different means (capacitive, resistive, optical, etc.) and mapping this data to relevant forces, an SEA is different in terms of its compliance which is orders of magnitude lower than typical force sensors: At the macro scale, a typical force sensor has a stiffness on the order of $10^7\ N/m$, while for example the SEA in [21] have a stiffness on the order of $10^3\ N/m$.

Another benefit of SEAs, include low overall the impedance of the system at the frequencies above the control bandwidth which avoids hard impacts with environment [22]. The main disadvantage of SEAs is their low control bandwidth due to the intentional introduction of the soft coupling element [23]. The force resolution of an SEA improves as the coupling is made more compliant; however, increasing compliance decreases bandwidth of the control system, trading off response time for force accuracy.

Advantages of SEAs, such as the ones presented in the previous paragraphs, have been well-recognized at macro scale since early 1990s [23] and these devices have been utilized in various applications, including exoskeletons [24, 25], prosthetic devices [26], and legged robots [27, 28]. Design challenges of SEAs have been studied in [29–31], while control challenges of these devices have been addressed in [22, 23, 32, 33].

In Table 1.1 popular SEA examples has been shown.

Table 1.1: Series elastic actuator examples

Name	Application Area	
LOPES (Twente)	Rehabilitation	
Electric SEA (Yobotics)	General purpose	
RoboWalker (Yobotics)	Exoskeleton	

1.3 Contribution of This Thesis

This thesis introduce a robust optimal design framework and a non-overshooting controller design for a micro-telemanipulation system which is based on series elastic actuation. The contributions of this work are:

- *Series elastic actuation method is proposed for force controlled micro-manipulation.* Even though SEA is a well-known used actuation method for force controlled manipulation in macro scale applications, it has not been taken advantage in micro-manipulation. This thesis deliberately introduces the SEA method to micro manipulation literature.

- *A robust multi-objective optimal design framework is introduced and mechanical design of a μSEA is performed using the proposed framework.* The proposed robust optimal design framework fuses a multi-criteria optimization method, namely Normal Boundary Intersection (NBI) method, with the robust optimal design method, called sensitivity region. The proposed design framework is advantageous in two ways: first, it simplifies the multi-criteria optimization into a geometric problem and solves it efficiently, second, the robustness is embedded into optimization procedure; therefore, the need for statistical data about the design variations and the need for measuring the sensitivity through the computation of the derivative of the objective functions are eliminated.

  The proposed design method is used to design the elastic coupling of the μSEA since the performance of the overall system highly depends on this part. A compliant, under-actuated half pantograph mechanism is chosen as the underlying kinematic structure of the μSEA. This se-

lection introduce an inherent robustness to manufacturing errors, while improving the accuracy of the motion of the mechanism which has a self-aligning end effector. According to manipulability and stiffness criteria, a reliable and optimal design is conducted.

- *A novel approach to force control problem of μSEA is introduced by synthesizing a non-overshooting controller which will satisfy a force response with reference input traced from below.* In the literature, there exist controllers synthesized for SEA based mostly on PID. In this work, a controller with non-overshooting response characteristic is designed for μSEA. The non-overshooting controller is based on backstepping controller and it preserves its non-overshooting response as an inherent featureindependent of the initial conditions of the system.

- *The optimally designed robust μSEA with its non-overshooting controller is implemented in a scaled bilateral micro-telemanipulation architecture so that a human operator can perform micro manipulation with force feedback.* The important aspect of the teleoperation structure is that while the master device is a rigid robot, the slave manipulator is a soft robot. As it has been shown in the literature, this hard-soft teleoperation structure improves the stability of the teleoperation system. Moreover, the slave side of the telemanipulation system preserves the non-overshooting response characteristic of the μSEA during interactions with the environment.

- Finally, the μSEA and the scaled telemanipulation system are implemented and characterized.

Chapter II

2   Hardware Design of the μSEA

The Series Elastic Actuator (SEA) system consists of the following components: actuator, spring, position sensor and a controller. A schematic representation of a generic SEA can be seen in Figure 2.1. The position sensor in the system is mounted on the elastic element to measure the deflection on the element where the force of the actuator that is exerted on the load is proportional to this deflection. This measurement is used in the feedback loop and fed to the controller of the system.

The design of the μSEA depends on the design of the elastic element, *i.e.* the spring, since the other parts of the device is chosen from the off-the-shelf items. This section introduces the design of the elastic element and the μSEA device.
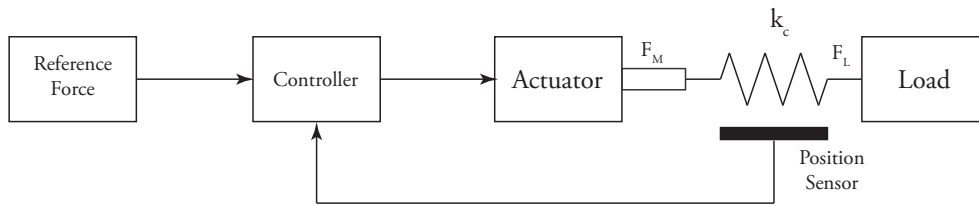

Figure 2.1: A generic series elastic actuator

This chapter is organized as follows: in the first section, the type selection of the elastic element is introduced. After deciding the mechanism

type, kinematic analysis is performed in order to mathematically express the performance measures, such as manipulability and stiffness. In the kinematic analysis, the use of pseudo-rigid body method is thoroughly introduced and mathematical formulations of the manipulability and stiffness are given. Once the performance metrics are formulated, the optimal dimensioning of the mechanism for the best performance is conducted. In the optimal dimensioning step, the performance of the mechanism and the reliability of the design are considered simultaneously.

2.1   Type Selection

The first step of the design is to decide on the fundamental characteristics of the system. Later on the design steps, these fundamentals will be considered in the optimal dimensioning step where the aim is to find the optimal design variables that improve the performance according to the optimization objectives.

The elastic element is the most important part of the μSEA which directly affects its performance. Therefore, it should be designed carefully. The very first thing in the selection of the elastic element is the lack of micro level helical springs which are widely used in the series elastic applications in the macro level. Since manufacturing a linear, helical spring is quite challenging for a microsystem, a simple, cost effective solution is needed. The commonly used spring like elements in the microsystems are the compliant mechanisms which are single piece, monolithic structures that gain their mobility though the deflection of their flexible links.

There are many advantages of using a compliant mechanism. For the practical purposes of μSEA design, the main advantage of a compliant mech-

anism is its spring like behavior. Consequently, the elastic element of the μSEA is chosen as a compliant mechanism. Besides the spring like behavior, using a compliant mechanism improves the quality of the operation and the control by eliminating the friction and backlash problems. Another important advantage of a compliant mechanism is that the designed mechanism in macro level can be scaled into micro level without making major adjustments. The compliant mechanism has tendency to stay in its initial configuration (the stable configuration), therefore energy storage is possible with compliant mechanism by keeping the system under deflection.

Although compliant mechanisms offer certain advantages, there are some drawbacks which cannot be ignored. Analysis of a compliant mechanism is more intricate than a rigid body mechanism. Due to the deflection of the links of the system, different modeling approaches like finite element modeling (FEM), assumed mode analysis (AMA) or pseudo-rigid body method should be used. Moreover, the stiffness of the compliant mechanism in its end effector coordinates is not linear and it requires aptitude for obtaining analytical expression for it. Compliant mechanisms have limited dexterous workspace compared to their rigid-body counterparts. Hence the design of a compliant mechanism should be carefully handled with a special care on the workspace.

To implement the compliant element of the μSEA, we choose a parallel mechanism based design. Parallel mechanisms are advantageous to use, for instance they offer robustness to manufacturing errors and dimensional changes due to thermal noise [34]. It should be noted here that, the reliability concerns on the μSEA design is first encountered in this step of the type selection and by choosing a parallel mechanism the reliability of the

design is improved. As it comes to the other advantages, the errors at the joint space of a parallel mechanism are averaged at the task space; therefore, parallel mechanisms can achieve more precise motion than their serial mechanism counterparts. Moreover, parallel mechanisms can be designed to be more compact with higher stiffness, compared to serial mechanisms [34]. Although dynamics of a body in micro level is negligible, the use of a parallel mechanism reduces the effective inertia of the system and it enables to ground the actuators.

The most significant difficulty of a parallel mechanism is the analysis of the system. The kinematics of a parallel mechanism requires elaborate analysis. It requires more computational power and, for most cases, it is not possible to obtain an analytical solution. The dexterous workspace of a parallel mechanism is incapacitated compared to a serial mechanism. Moreover, there may be many singularities in the workspace of the parallel mechanism; therefore, a fine singularity analysis should be conducted.

In particular, a half pantograph mechanism with 3 degrees of freedom (DoF) is selected as the underlying kinematic structure of the compliant element. The half-pantograph is driven by a single actuator; therefore, the μSEA is under-actuated. The under-actuation is intentionally built into the μSEA design, since it introduces reliability and robustness by passively compensating the alignment errors of the actuator and the end effector. The under-actuation also helps with the impact-resistance of the device.

Figure 2.2 depicts a schematic representation of the mechanical design of the μSEA with compliant half-pantograph based elastic elements where the solid line represents the initial configuration of the μSEA and the dash line is the configuration due to actuation. In the figure, the actuator is

located in between two half-pantograph mechanisms. This configuration is especially suitable for use with low cost piezoelectric actuators with screw motions, since the actuator can simply be placed in position and kept there by pre-loading the elastic elements. The compliant mechanisms of the μSEA is installed to the actuator with preload so that a clearance free assembly is achieved. In the figure, the end effector is assumed to be a microprobe suitable for manipulation.
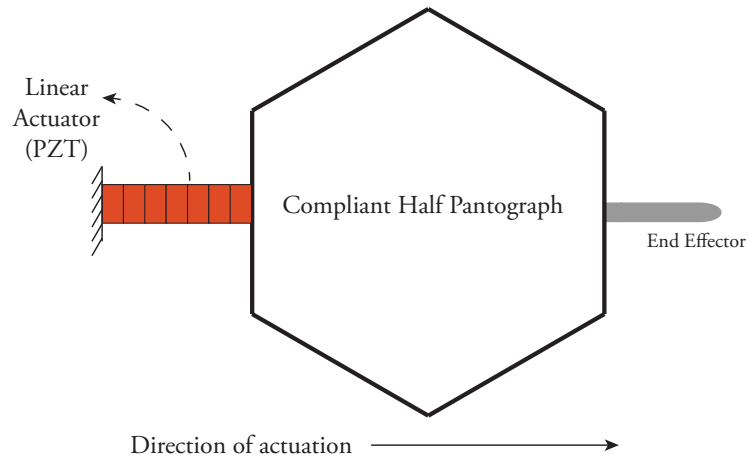
Figure 2.2: Schematic representation of the μSEA

2.2 Kinematic Analysis

The analysis of compliant mechanisms is significantly harder than the analysis of their rigid body counterparts, since the study of these mechanisms require the determination of their deformations under externally applied forces. In this thesis, an approximate model, namely the pseudo-rigid body model [35], is used to study the kinematics of the compliant half-pantograph mechanism. Pseudo-rigid body model is preferred due to its computational efficiency and ease of use.

A pseudo-rigid body approximates the motion of a compliant mechanism by replacing its flexible links with rigid links and introducing torsional springs at both ends of these rigid ones. The torsional springs mimic the flexibility of the system while the introduction of rigid links enable the use of rigid body mechanics. Link lengths and spring constants in the model are selected such that the kinematics of the model closely approximates the solution of elliptic integrals that arise from the exact solution of the compliant link deformations. While the accuracy of the pseudo-rigid body method depends on many parameters, such as the length of the flexible members, for small pivot movements with relatively long link lengths, as studied in this paper, the approximate solution lies within 0.5% percent of the exact solution [36].
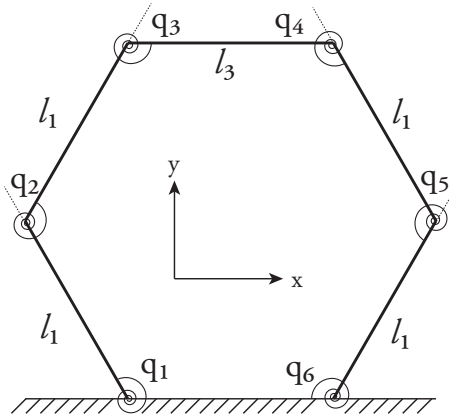
Figure 2.3: Pseudo-rigid body model of the half-pantograph mechanism

Figure 2.3 depicts the pseudo-rigid body model of the half-pantograph mechanism. The joint angles are chosen to be the generalized coordinates of the system. The generalized coordinates, q, are categorized as active, q_a, and passive, q_p, ones: an active generalized coordinate corresponds to the orientation of a joints that is actuated, while a passive generalized coordinate

pertains to the orientation of an hindered joint.

$$q = \begin{bmatrix} q_a \\ q_p \end{bmatrix} = \begin{bmatrix} q_1 \ q_6 \ | \ q_2 \ q_3 \ q_4 \ q_5 \end{bmatrix}^T \tag{1}$$

The Jacobian matrix of the system is also partitioned into kinematic Jacobian J_T, which gives the relation between the joint space and task space velocities, and constraint Jacobian J_C, which imposes the motion constraints to the system.

$$\dot{x} = J_T(q)\dot{q} \tag{2}$$

$$0 = J_C(q)\dot{q} \tag{3}$$

The kinematic and constraint Jacobian matrices are then grouped by the type of the joint. This new form of the Jacobian matrix provides more insight about the system, since the sub-blocks of the matrix clearly reflects the contributions of the active and passive joints.

$$\begin{bmatrix} \dot{x} \\ 0 \end{bmatrix} = \begin{bmatrix} J_{T_a} & J_{T_p} \\ J_{C_a} & J_{C_p} \end{bmatrix} \begin{bmatrix} \dot{q}_a \\ \dot{q}_p \end{bmatrix} \tag{4}$$

The compliant half-pantograph is under-actuated since the number of driven joints is less than the degrees of freedom of the system. The under-actuated nature of the mechanism increases the complexity of the kinematic analysis. However, the under-actuated compliant half pantograph mechanism obeys the Hamilton's principle, therefore, it can be stated that the motion of the pantograph will minimize the strain energy in its passive joints. Such an approach is also adopted in [37]. This new optimization problem can be

19

formulated as

$$\arg\min_{\dot{q}_p} \frac{1}{2}\dot{q}_p^T K_{q_p}\dot{q}_p \quad \text{subject to} \quad J_{C_a}\dot{q}_a + J_{C_p}\dot{q}_p = 0 \tag{5}$$

where K_{q_p} is the stiffness matrix of the passive joints. This new problem minimizes the strain energy of the passive joints while satisfying the closed kinematic chain constraint of the half pantograph. The optimization problem can be solved using the method of Lagrange multipliers.

$$\mathcal{L} = \frac{1}{2}\dot{q}_p^T K_{q_p}\dot{q}_p + \lambda^T(J_{C_a}\dot{q}_a + J_{C_p}\dot{q}_p) \tag{6}$$

Minimizing Equation 6 yields to the relation between the passive and active joint velocities.

$$\dot{q}_p = -(K_{q_p} + K_{q_p}^T)^{-1}J_{C_p}^T[J_{C_p}(K_{q_p} + K_{q_p}^T)^{-1}J_{C_p}^T]^{-1}J_{C_a}\dot{q}_a. \tag{7}$$

Substituting Equation 7 into the Jacobian of the system (Equation 4), the mapping between the task space velocities and the active joint velocities can be uniquely derived as

$$\dot{x} = (J_{T_a} - J_{T_p}J_{C_p}^{\ddagger}J_{C_a})\dot{q}_a = \bar{J}_T\dot{q}_a \tag{8}$$

where $J_{C_p}^{\ddagger} = (K_{q_p} + K_{q_p}^T)^{-1}J_{C_p}^T[J_{C_p}(K_{q_p} + K_{q_p}^T)^{-1}J_{C_p}^T]^{-1}J_{C_a}$.

2.3 Optimal Dimensional Synthesis

2.3.1 Performance Metrics

The performance trade-offs that exist during the design of μSEAs need to be handled systematically so that the best possible force tracking performance can be achieved. In this section, given the half-pantograph mechanism as the underlying kinematics of the compliant element, an optimal dimensional synthesis problem is formulated. The dimensional synthesis problem is critical especially for parallel mechanism, since small changes in these parameters can have crucial effects on the overall performance of the mechanism [34].

Most important aspect of the compliant mechanism is its stiffness, which lets it act as a spring. In general, compliant mechanisms have configuration dependent task-space stiffness at their end-effectors. While designing a μSEA the task stiffness of the mechanism needs to be optimized for the accuracy and reliability of force control. Hence, task space stiffness is the first metric to be included in the optimization problem.

The compliant mechanism used in the μSEA is implemented as a flexure joint mechanism, in which deflections can only occur at the corners of the mechanism where two rigid links articulate. Since the deflection of these joints are limited, the dexterous workspace of the mechanism is drastically reduced compared to a traditional rigid body mechanism of the same kinematics. One of the important design goals for the μSEA is increasing the dexterous workspace of the device so that a wider range of operation becomes feasible. In order to characterize the size of the dexterous workspace, manipulability [38] is used as the second metric for the optimization problem.

Two metrics (stiffness and manipulability) need to be optimized for the

half-pantograph mechanism while implementing the μSEA. However, the half-pantograph possesses 3DoF in plane and it is more proper to conduct the analysis along different directions, in other words, consider the directional manipulability and stiffness of the mechanism. The analysis considers two mutually perpendicular directions: direction of actuation (y-direction), and the direction that is perpendicular to it (x-direction). Along the direction of actuation, the end effector of the μSEA contacts with the environment, *i.e.* it is the active direction; while no motion is desired along the perpendicular direction. These directions can be seen in Figure 2.2.

In particular, we analyze the manipulability and the stiffness of the mechanism along the direction of actuation and along the direction perpendicular to its motion as follows: We increase the manipulability and decrease the stiffness of the mechanism along the movement direction of actuation to achieve high stroke with high force resolution, while we decrease the manipulability and increase the stiffness of the mechanism along the direction perpendicular to the actuator motion to achieve good disturbance rejection characteristics.

The manipulability and the stiffness metrics are equivalent for the half-pantograph mechanism, that is, both performance criteria converge to the same optimal dimensions for the mechanism. Decreasing stiffness and increasing manipulability yields a long mechanism with the link lengths at their upper limits, while increasing the stiffness and decreasing the manipulability converges to a short mechanism with the link lengths at their lower limits. Due to this equivalence, it is unnecessary to distinctly analyze the stiffness and the manipulability metrics; hence, only the stiffness along the x- and y-directions are examined during optimization.

After the optimization metrics are defined, one can use the kinematics of

the system to formulate each objective function so that an optimal dimensioning can be performed. The only performance metric that will be used is the stiffness of the system. Therefore, it is required to have an analytical expression of the task space stiffness of the system. Once the kinematics of the system is known, the task space stiffness of the mechanism can be calculated as

$$K_T = \bar{J}_T^{-1}(K_{q_a} + J_{C_a}^T J_{C_p}^{-T} K_{q_p} J_{C_p}^{-1} J_{C_a})\bar{J}_T.$$ (9)

In the optimization problem, directional stiffness is analyzed along two different directions: x- and y-directions (refer to Figure 2.3). Stiffness of the compliant half-pantograph mechanism; hence; the optimization metrics can be calculated as

$$\mu_{S_x} = u^T K_T u$$ (10)

$$\mu_{S_y} = v^T K_T v$$ (11)

where u and v represent the unit vectors in the x- and y-directions, respectively.

The negative null form of the optimization problem can be formulated as,

$$\arg\max_{\alpha} \mathbf{F}(\boldsymbol{\alpha}, \boldsymbol{\beta}) \quad \text{subject to}$$

$$\mathbf{G}(\boldsymbol{\alpha}, \boldsymbol{\beta}) \leq 0 \quad \text{and}$$ (12)

$$\boldsymbol{\alpha}_l \leq \boldsymbol{\alpha} \leq \boldsymbol{\alpha}_u$$

where α represents the vector of design variables –the link lengths and the pose of the mechanism $\alpha = [\ell_1 \ \theta]^T$– and β denotes the design parameters – not available in this problem. In this negative null form, $\mathbf{F}(\boldsymbol{\alpha}, \boldsymbol{\beta})$ is the

23

vector of performance metrics. For this optimal design problem: $\mathbf{F}(\boldsymbol{\alpha}, \boldsymbol{\beta}) = [\mu_{S_x} \ \mu_{S_y}]^T$, where μ_S represents the task space stiffness. $\mathbf{G}(\boldsymbol{\alpha}, \boldsymbol{\beta})$ is the vector of inequality constraints. The inequality constraints are imposed during the kinematic analysis to ensure a closed kinematic chain and elbow out posture of the half-pantograph mechanism.

2.3.2 Normal Boundary Intersection Method (NBI)

In general, introducing one more objective function into an optimization problem increases the complexity. Most of the time, the optimal solution of one objective function will not be an optimal solution with respect to another objective function, especially if those optimization metrics are conflicting with each other. Therefore, instead of optimizing the objective functions independent of each other, a solution procedure that can handle multiple objective functions simultaneously should be used.

The optimization problem, which includes more than one objective function, can be attacked using two different approaches, namely scalarization and Pareto methods. Scalarization methods transform multiple objective functions into a single performance metric by aggregating/prioritizing these functions. The fundamental disadvantage of scalarization approaches is that, the weight/priority of each objective needs to be assigned a priori, in other words, the best choice of the weights/priorities, which can only be determined after the optimization procedure is complete, is demanded before the optimization procedure is initialized. An improper choice of the weights/priorities may yield to an unsatisfactory optimal solution.

Unlike scalarization approaches, Pareto methods do not require a priori information about the design trade-offs, instead they try to characterize

these trade-offs among multiple objective functions. In this study, the multi-criteria optimization problem is solved using Pareto methods, in particular, utilizing the framework introduced in [39–41]. The framework proposes using the Normal Boundary Intersection (NBI) method to obtain efficient solutions for the multi-criteria optimization of parallel mechanisms.

The NBI method is one of the robust methods to obtain the design trade-offs (the boundary of the feasible domain) of multi-objective optimization problems [42]. The NBI method uses a geometric approach to solve for the optima of the multi-objective problems. In particular, the NBI method performs a sequence of gradient-based searches on the feasible domain defined by the problem. The method is computationally efficient, since it attacks the geometric problem directly and solves for single-objective constrained subproblems using fast, reliable gradient-based optimizers. Because the geometric problem is only affected by the properties of the feasible domain, the single-objective subproblems can be addressed using gradient based optimization techniques, even when the objective functions are non-smooth and non-convex. Moreover, the method is applicable to a general set of performance indices and results in exceptionally uniform distributed points on the Pareto-front hyper-surface without requiring any tuning of the core algorithm.

Limitations of the technique exist since the NBI method relies on an equality constraint. It is possible for the NBI method not to find a solution on the Pareto-front hyper-surface or converge to a local optima. In such a case, the solutions of NBI subproblems can be post-processed to filter out undesired dominated solutions. Moreover, NBI method assumes sufficient smoothness of the boundary of the feasible domain so that gradient techniques can be

employed. However, it has also been demonstrated in the literature that the method performs remarkably well even for non-smooth geometries of the objective space [43].

This multi-criteria optimization, NBI, is used to optimize the performance of the μSEA with respect to the stiffness objectives. The solution of the multi-criteria optimization, *i.e.* the Pareto front curve, can be found in Figure 2.4. This optimization procedure does not consider the possible deviations in the optimization variables that may occur during implementation. Hence the link length and the initial pose found during the optimization are nominal values. In order to guarantee the reliability of the system due to the unexpected changes in the optimization variable, the optimization framework should explicitly consider the robustness. The reliability based design is introduced in the next section, 2.4.

2.4 Robust Optimal Design

In this section, the robust optimization method proposed by Gunawan and Azarm [44] is utilized to extend the optimal dimensional synthesis framework introduced in [41, 45] to incorporate robustness into the design. The aim of the robust optimization is to find design variables for the mechanism such that the objective function value is less sensitive to the deviations in the design variables.

2.4.1 Single Objective Robust Optimal Design

The NBI method used to solve the multi-criteria optimization problem requires to be initialized with the solutions, called shadow points, that minimize each objective function individually. To determine the optimum of each ob-
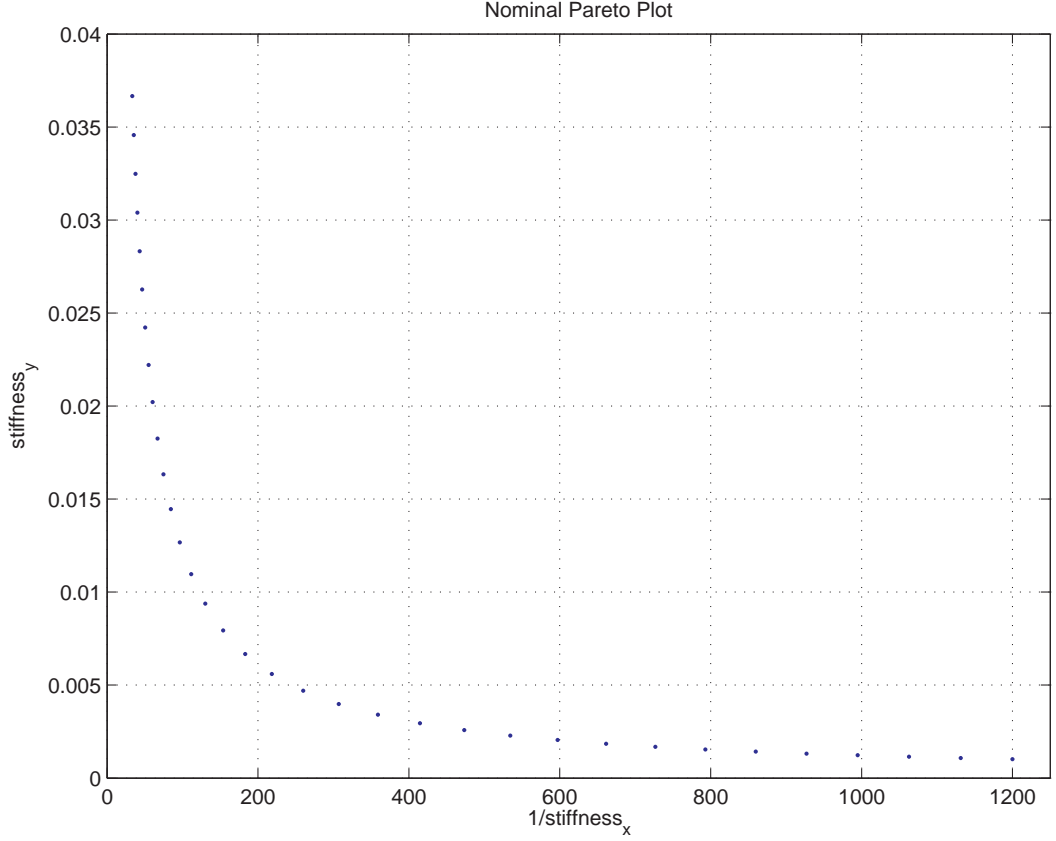
Figure 2.4: Pareto front curve of the multi-criteria optimization problem

jective function, a single objective optimization problem needs to be solved for each criteria. Since we are interested in robust designs, a robustness criteria should be added to this optimization problem so that performance can be guaranteed under variations of the design variables.

To ensure robustness, the key concept of the sensitivity region is defined as,

$$S(x_0) = \left\{ \Delta \mathbf{x} \in \mathbb{R}^N \mid [f(\mathbf{x}_0 + \Delta \mathbf{x}) - f(\mathbf{x}_0)]^2 \leq [\Delta f_0]^2 \right\} \qquad (13)$$

where $\Delta \mathbf{x}$ is an N dimensional vector of variations of design variables and Δf_0 is the maximum allowed change in the objective function to be determined

27

by the designer. The sensitivity region represents a set, where the changes in the function value due to the deviations from the nominal values of the design variables by an amount of $\Delta\mathbf{x}$ remains less than or equal to Δf_0. In general, the sensitivity regions have an arbitrary shape rendering its computation ineffective. Moreover, the combination of deviations in the design variables cannot be foreseen during the design step. To address these challenges, a conservative and simple approximation to the sensitivity region is proposed in [44]. In particular, the largest hyper-sphere that tightly fits inside the sensitivity region is considered and the radius of this hyper-sphere, that is also the closest point to boundary of the sensitivity region to the origin of the variation space, is proposed as a measure of robustness. This radius can be calculated as the solution of the following optimization problem.

$$\underset{\Delta\mathbf{x}}{\arg\min} \quad R(\Delta\mathbf{x}) = ||\Delta\mathbf{x}||_2 \tag{14}$$

$$subject\ to \quad \frac{\Delta f_0^2}{(f(\mathbf{x}_0 + \Delta\mathbf{x}) + f(\mathbf{x}_0))^2} - 1 = 0$$

In this new optimization problem, the constraint imposes that the solutions lie on the boundary of the sensitivity region.

Introducing the robustness criteria into the single optimization problem to calculate the shadow points transforms this problem into a multi-objective optimization, where the objective function and the robustness of the system have to be optimized simultaneously. However, in order to simplify the analysis, it is convenient to consider the robustness condition as a constraint to the single optimization problem. In particular, the optimization problem can be constrained to have solutions that satisfy some predetermined robustness index, R_0. The negative null form of the single optimization problem with

robustness constraint can be formulated as

$$\arg\min_{\alpha} \quad f(\alpha, \beta)$$
$$\text{subject to} \quad \mathbf{g}(\alpha, \beta) = 0$$
$$\mathbf{h}(\alpha, \beta) \leq 0 \qquad (15)$$
$$\alpha_L \leq \alpha \leq \alpha_U$$
$$R_0 - R < 0$$

Even though considering the robustness condition as a constraint avoids a multi objective problem, choosing a proper value for R_0 is not trivial. In [44] using $R_0 = \sqrt{N}$, where N is the number of design variables in the optimization problem, is suggested as a proper choice for R_0. For further details of this choice and the theory behind the robust optimization technique, readers can refer to [44].

2.4.2 Multi Objective Robust Optimal Design

In [46], the robustness criteria based on sensitivity region is extended to multi-criteria optimization problems. In particular, it is shown that the concept can be incorporated into Multi-Objective Genetic Algorithm (MOGA) [47] after some minor tuning. In this study, we follow a similar formulation but utilize the NBI method to solve the multi-criteria optimization problem, since it is one of the most efficient methods to solve for the design trade-offs [47]. Compared to MOGA [47] that requires problem dependent fitness search related tuning and several steps to reach convergence, a standard NBI approach can map the Pareto front hyper-surface with higher accuracy and uniformity, while also inheriting the efficiency of gradient-based methods.

Benefits of NBI method over MOGA has been observed in many studies, including [43].

The multi-criteria optimization problem with robustness constraint can be formed as

$$
\begin{aligned}
\arg\min_{\alpha} \quad & \mathbf{F}(\alpha, \beta) \\
\text{subject to} \quad & \mathbf{g}(\alpha, \beta) = 0 \\
& \mathbf{h}(\alpha, \beta) \leq 0 \\
& \alpha_L \leq \alpha \leq \alpha_U \\
& R_0 - R < 0
\end{aligned}
\tag{16}
$$

where R is determined as the solution of the following optimization problem

$$
\arg\min_{\Delta\mathbf{x}} \quad R(\Delta\mathbf{x}) = ||\Delta\mathbf{x}||_2 \tag{17}
$$
$$
subject\ to \quad \max_{i=1,...,M} \left(\frac{|f_i(\mathbf{x}_0 + \Delta\mathbf{x}) + f_i(\mathbf{x}_0)|}{\Delta f_{i,0}} \right)^2 - 1 = 0
$$

where $\mathbf{F}(\mathbf{x}) = [f_1(\mathbf{x}) \dots f_M(\mathbf{x})]$ is the vector of objective functions and $\Delta f_{i,0}$ is the maximum allowed variation in each objective function.

2.5 Design Selection from the Pareto Front

In this design problem, the performance and the reliability is being achieved by changing the link length ℓ_1 and the initial posture of the mechanism, θ. The design variables can be seen in Figure 2.3.

$$
\mathbf{x} = [\ell_1\ \theta]^T \tag{18}
$$

30

Due to the constraints on the raw material that can be used in the manufacturing, the design variables have lower an upper bounds:

$$10 \ mm \leq \ell_1 \leq 60 \ mm \tag{19}$$

$$10° \leq \theta \leq 60° \tag{20}$$

The design of the elastic element is conducted using the design framework which is introduced in the previous sections. In this analysis, $\mathbf{\Delta x}$ represents the variation on the variables. For 4 different variations, the Pareto front is calculated.

$$
\begin{aligned}
\mathbf{\Delta x_1} &= \begin{bmatrix} 0.1mm & 0.1° \end{bmatrix} \\
\mathbf{\Delta x_2} &= \begin{bmatrix} 0.5mm & 0.5° \end{bmatrix} \\
\mathbf{\Delta x_3} &= \begin{bmatrix} 0.75mm & 0.75° \end{bmatrix} \\
\mathbf{\Delta x_4} &= \begin{bmatrix} 1mm & 1° \end{bmatrix}
\end{aligned}
\tag{21}
$$

In order to observe the shift in the Pareto, in other words view the trade-off between the performance and reliability, the nominal Pareto front, which does not have any robustness constraint, and the robust Pareto fronts are given in the same figure (refer to Figure 2.5). It is clear from the figure that, as the variations in the design variables increases (in this case they vary from $[0.1mm \ 0.1°]$ to $[1mm \ 1°]$) the Pareto front curve shifts towards into the feasible region by becoming a dominated solution.

In Figure 2.5, the Pareto curve of $\mathbf{\Delta x_4}$ is clearly distinct from others. However, it can be observed that, the Nominal Pareto front and the robust Pareto fronts of $\mathbf{\Delta x_1}$, $\mathbf{\Delta x_2}$ are overlapping. This is due to the inherent
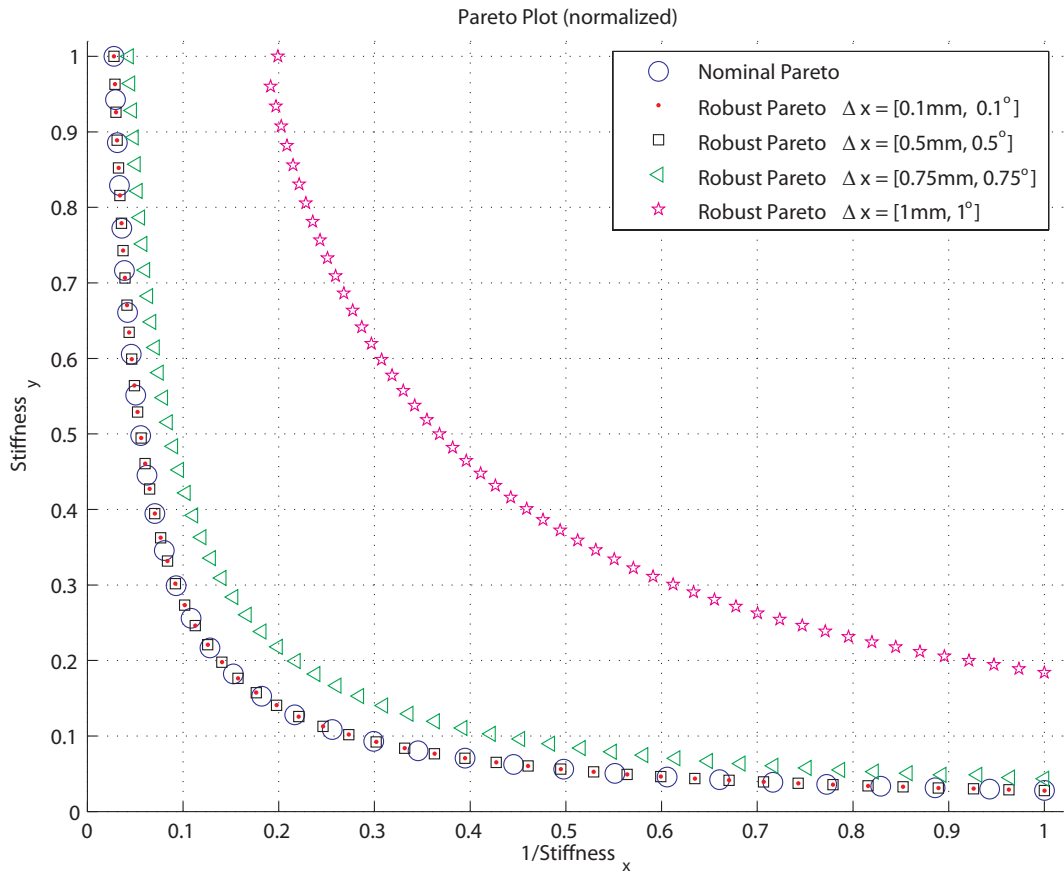
Figure 2.5: Normalized Pareto front curves for nominal and robust designs

robustness of parallel mechanisms. As it is stated in the "Type Selection" step, parallel mechanisms can compensate errors such as the ones occur in manufacturing or thermal noise. Due to this inherent reliability of the system, the first three variations do not significantly degrade the performance of the design, *i.e.* the Pareto curve do not shift.

This pantograph mechanism will be manufactured using wire-EDM method. In this method the raw material is cut using a wire with a diameter of 0.25mm. The manufacturing tolerance of a wire erosion is $1\mu m$. Therefore, the rest of the analysis will be conducted using the first robust Pareto

curve (the one with the variation Δx_1). The denormalized Pareto front can be seen in Figure 2.6.
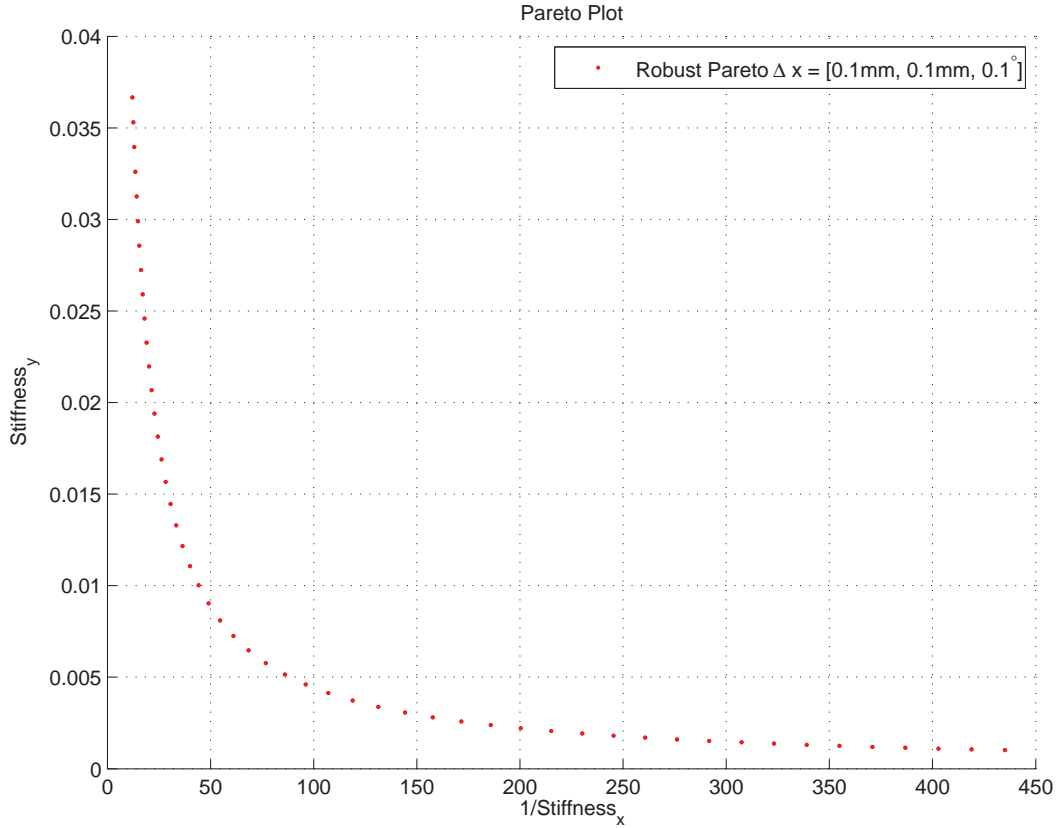
Figure 2.6: Denormalized Pareto front curve for $\mathbf{\Delta x_1} = [0.1mm \quad 0.1°]$

On the Pareto curve there are many solution which minimizes the objective functions, stiffness in the x- and y-directions, simultaneously. In this set of solutions one final configuration should be chosen as the elastic element. This choice can be made by considering many criteria not restricted by the optimization metrics. In this design problem, the election of the final design is made by considering the footprint and the y-direction stiffness of the mechanism. Before going into the details of the selection one thing

should be emphasized. The footprint constraint is not as important as the optimization metrics, hence it is not included in the optimization problem. Doing so leads to a broader perspective of solutions where the optimality is due to the criteria that is crucial according to the quality of the design. Once the solution set is obtained, a final configuration is chosen using the criteria including the less crucial ones.

In this design problem, the footprint of the criteria is a second degree criteria therefore it is embedded into the analysis after obtaining the Pareto front. The footprint criteria is identified according to the raw material that is available to manufacturing. This criteria states that the maximum area of the mechanism should be less than 2000mm^2. The points with black dots in Figure 2.7 do not satisfy this condition.

On the other hand, since this elastic element will serve as the spring of the μSEA, it is important to have low stiffness along the actuation direction so that the force resolution of the μSEA will be better. The second elimination criteria is the stiffness of the compliant element which is desired to be lower than 0.01Nmm/rad. This criteria eliminates the points marked with black boxes in Figure 2.7. The rest of the points, shown in red pentagram in Figure 2.7 satisfy not only the performance issues imposed into the optimization problem, but also satisfy the less important criteria like the footprint. Among those points, the one with the lower y-direction stiffness is chosen as the final configuration for the elastic element of μSEA.
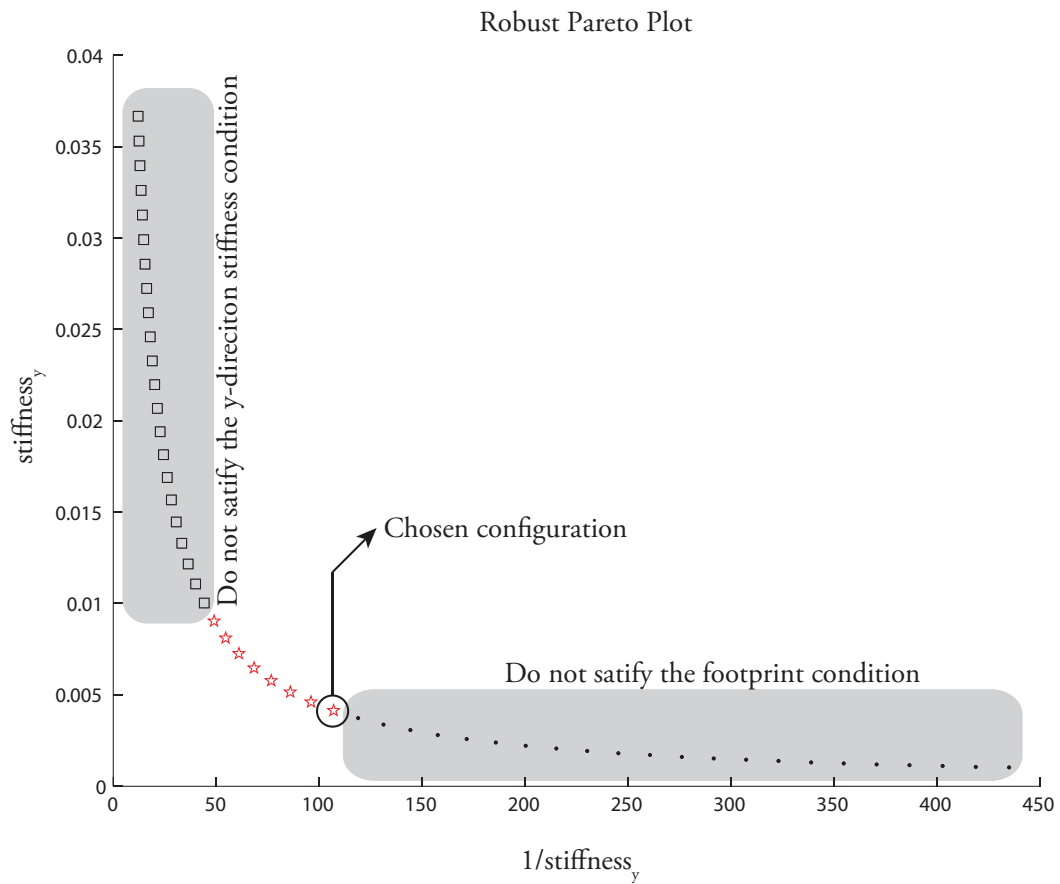
Figure 2.7: Point selection on the Pareto front curve

2.6 Realization of the Elastic Element

2.6.1 Solid Modeling of the Elastic Element

A CAD model for the pantograph with the link lengths and posture found in optimal dimensioning is created. Figure 2.8 depicts the front, bottom and right views of the half pantograph.
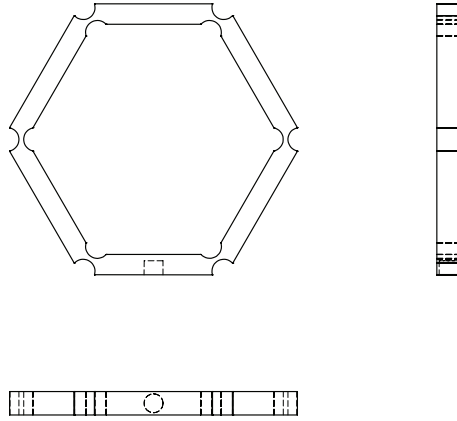
Figure 2.8: Solid model of the half pantograph mechanism

2.6.2 Flexure Hinges

As it is assumed in the analysis, the hinges of the mechanism are circular. For those circular hinges, Figure 2.9, the analytical form of the stiffness is read as [37],

$$K_\theta \approx \frac{2Ew}{9\pi}\sqrt{\frac{t^5}{R}} \qquad (22)$$
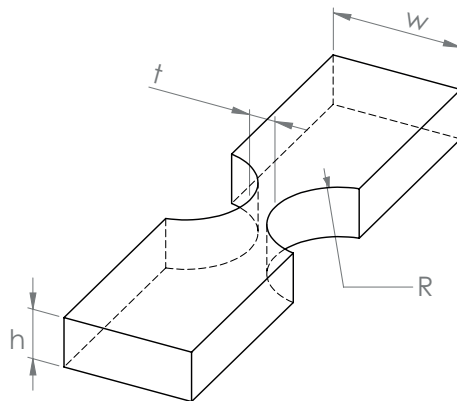
Figure 2.9: Circular hinge used in the pantograph

In this analytical model, Equation 22, E is the Young's modulus of the material, w is the width of the hinge, t s the minimum distance in the hinge,

and the R is the radii of the cavity. According to this model, the stiffness of each flexure hinge in the half pantograph of μSEA has a stiffness of $K_\theta = 11.072 \ Nm/rad$. The task space stiffness values of the pantograph mechanism with the flexure hinge, link length and initial pose presented here are: $K_{T_x} = 37.469 N/mm$ and $K_{T_y} = 45.795 N/mm$.

2.6.3   Finite Element Analysis of the Elastic Element

The half pantograph mechanism is analyzed using finite element method. The von Mises stress distribution of the deflected pantograph under 1 Newton of loading can be seen in Figure 2.10.
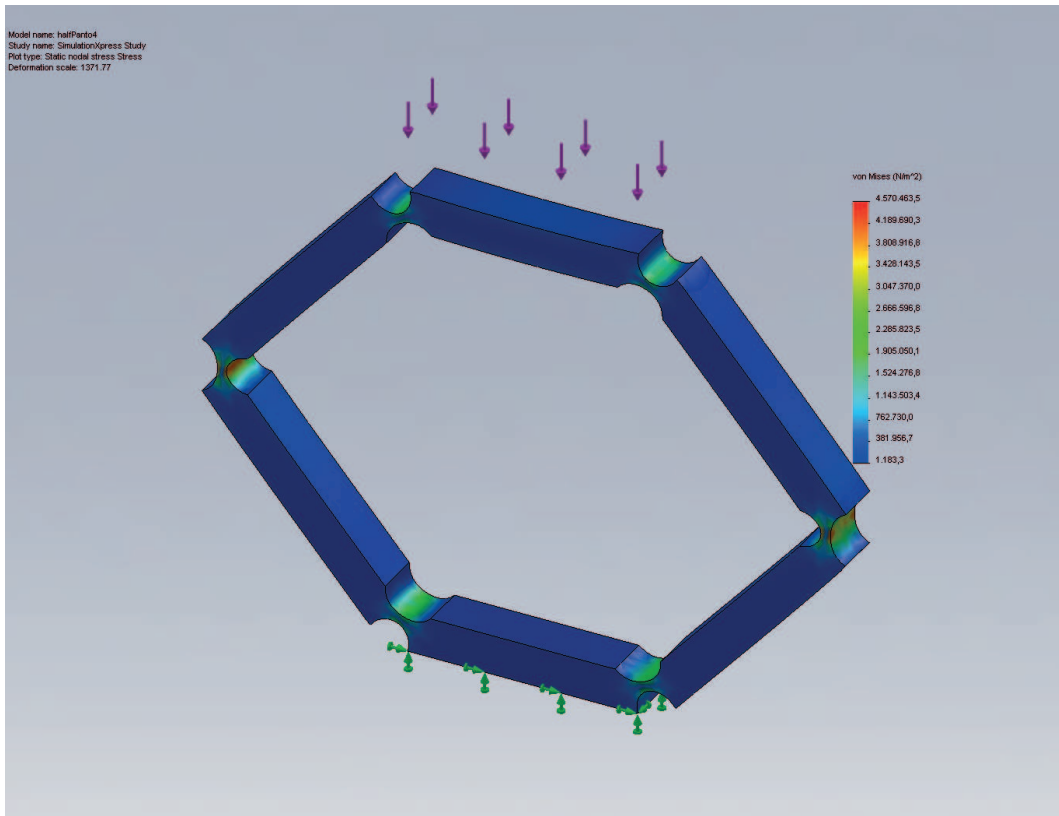

Figure 2.10: Stress distribution of the half pantograph under 1N of loading

As it is seen from the previous figure, the pantograph can withstand force around 1N. For this analysis, the factor of safety of the mechanism is greater than 10.

2.7 μSEA Setup

The hardware of the μSEA is a combination of the compliant half pantograph whose design is introduced previously, and a piezoelectric actuator. In order to control the deflection of the compliant coupling element a linear position sensor is mounted on the half pantograph. The details of the hardware and the components are given in the rest of the chapter.

The elastic coupling element of the μSEA Figure 2.11, is a compliant half pantograph which has been designed for better stiffness, manipulability and reliability. The design steps can be found in the previous sections of Chapter 2. This compliant mechanism is manufactured using wire-EDM method which has a tolerance of $1\mu m$.

The linear position sensor is mounted on the compliant mechanism in such a way that as the μSEA moves in free medium, the sensor will not generate signal since there is no deflection. However, is there occurs a deflection in the system position sensor directly measures the amount of deflection. The mounting of the linear encoder can be found in Figure 2.14.

The actuator, Figure 2.12, used in the system is a piezoelectric actuator of Piezomechanik company. It has a stroke of $13\mu m$ and it can supply forces upto 800N. Due to the limited stroke of the actuator, μSEA will have considerable low stroke but the the position resolution and the maximum attainable force characteristics of the μSEA due to the piezo actuator is good.

The sensor used in μSEA is the linear encoder (Tracker©) of New Scale

Technologies, Figure 2.13. It is a digital encoder and it consists of a chip and a magnet. The magnet has a layered structure of north-south pole pairs. As the magnet travels along the chip, a digital signal is generated due to this relative motion. As an advantage of the Tracker sensor is that it does not effected from light or vibration. It has a long travel range (up to 11mm) and supplies direct digital output.

In order not to have a clearence between the piezo actuator and compliant pantograph, and in order to have a self-standing device the piezo acuator and the compliant mechanism are coupled together with a preloaded half pantograph. This structure is adjoint to the compliant mechanism and it has not been subject to any optimization procedure. Its only aim is to create a preload that will keep the compliant mechanism and the piezo actuator together. The components of the μSEA in assembled form can be seen in Figure 2.14.
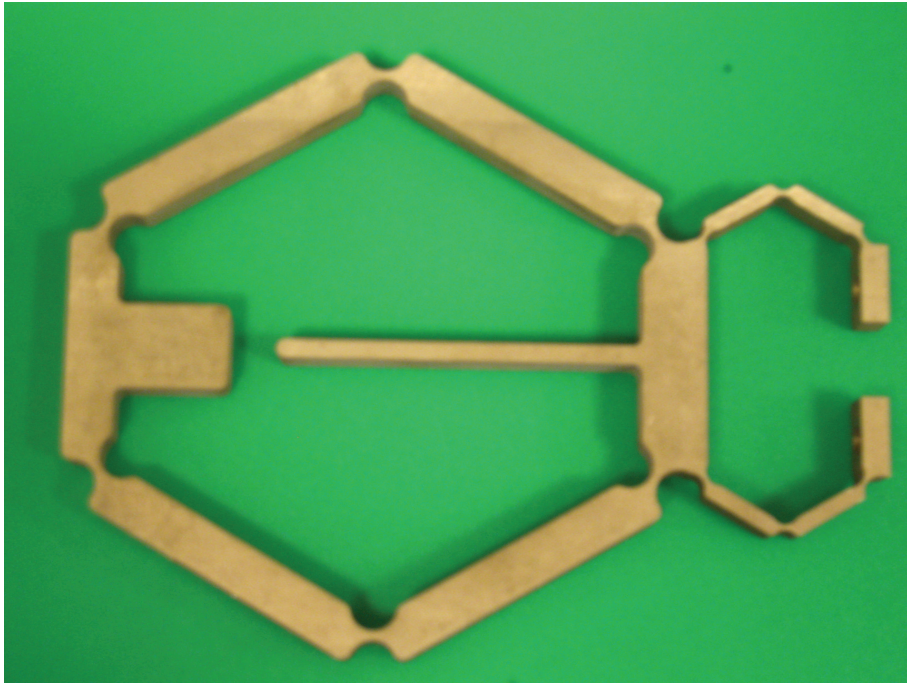
Figure 2.11: Elastic coupling element, *i.e.* half pantograph


Figure 2.12: Piezoelectric actuator
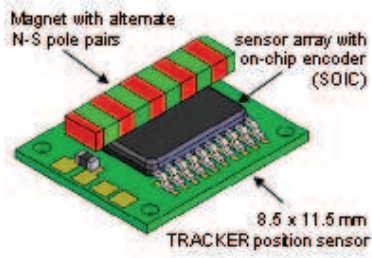
Figure 2.13: Linear position sensor
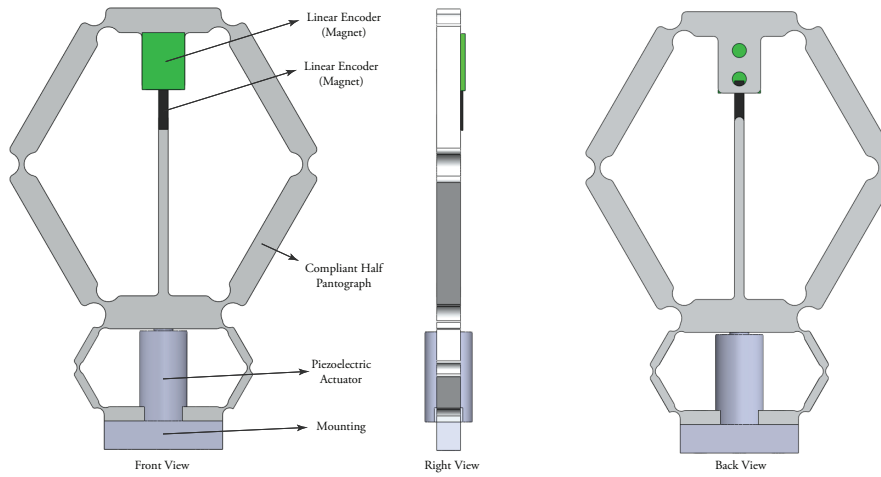
Figure 2.14: Micro series elastic actuator: piezo actuator, linear encoder and elastic element

Chapter III

3 Force Control and Scaled Teleoperation of Micro Series Elastic Actuator

The importance of the control of the force of a robotic manipulator can be easily understood in a cell manipulation example. Assume that the objective is to manipulate (hold or move) a living cells. Note that, although the cell membrane is considerably resilient, there is an amount of force that it can stay without damage. In this case, the manipulator that is performing the task should not only perform high quality positioning, but also be capable of controlling the contact force between the end effector of the manipulator and the cell. In such situations, force control strategies should be adopted.

As it is emphasized in *Introduction*, Series Elastic Actuator (SEA) is a delicate way of building a force controlled mechanism. The simplicity of its force–deflection relation enables the users to implement reliable and efficient position controllers to have reliable force controlled structure.

In this chapter, force control strategies used in series elastic actuators are presented in 3.1. A simple yet sufficient model of a series elastic actuator is given in Section 3.2. The nonovershooting control concept and the derivation of such a controller is given in 3.3.1. The SEA system with non-overshooting controller is embedded into a 3-Channel teleoperation architecture. The teleoperated manipulator system is discussed in 3.4.

3.1 Force Control Approaches in Series Elastic Actuators

In the literature, series elastic actuators have been controlled using various control methods, ranging from PID control to impedance control techniques. In [23], Pratt implemented a standard PID controller with feed-forward terms that are introduced to compensate for the nonlinearities of the input signal. In [48], Sensinger et. al. utilized impedance control for a SEA whose intrinsic impedance is low. Similarly in [49], Pratt et. al. used an impedance controller for a SEA and showed that voltage mode drive results in better performance than torque mode drive. In [32], Wyeth showed that a position loop can be placed inside the force control loop so that the motor can be treated as a pure velocity source and the design of the outer control loop can be simplified. In [33], Vallery et. al. used the control structure proposed by Wyeth, and proposed conditions to ensure the passivity of the SEA. In particular, a PI controller is used for the inner velocity loop while the outer loop is synthesized utilizing the passivity analysis.

3.2 Dynamic Model of a Series Elastic Actuator

The series elastic actuator can be simplified into a mass-spring system with a load attached to its end, this lumped mass-spring system can be viewed in Figure 3.1. The equations of motion for this system is,

$$m_M \ddot{x}_M = F_M - F_L \tag{23}$$

where the index "M" stands for motor, and similarly "L" stands for the load. The symbol m_M is the mass of the motor, F_M is the input to the system.
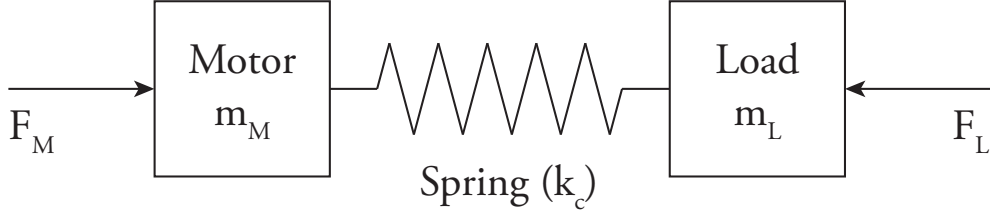
Figure 3.1: Mass-spring model of the series elastic actuator with load

The load force depends on the deflection of the motor spring. Therefore, it can be explicitly written as,

$$m_M \ddot{x}_M = F_M - k_C(x_M - x_L) \tag{24}$$

One thing should be emphasized here, the stiffness of the series elastic actuator, k_C, is not constant like a general spring since it is a compliant pantograph mechanism. The spring constant of the system is position dependent; therefore, it is a function of both the motor position, x_M, and the load position, x_L which acts like a disturbance on the system.

One aim of this thesis is to establish a nonovershooting controller for the μSEA. The synthesis of the nonovershooting controller can be easily conducted using state space approach. Therefore, this equation of motion, Equation 24, is transformed into state space form where the states are chosen as the position and velocity of the motor. The state space form of the equation of motion with this state choices is read as, (without loss of generality, it is assumed that there is no disturbance, *i.e.* load is stationary, on the

44

system.)

$$\dot{x}_1 = x_2$$
$$\dot{x}_2 = u + \frac{k_C}{m_M}x_1 \qquad (25)$$
$$y = k_C x_1$$

where $u = \frac{F_M}{m_M}$ is the control input to the system, x_1 is the state related to the motor position, x_2 is the speed of the motor, and y is the output of the system, that is the load force F_L. It should be pointed out that this state space model is of the form of strict feedback where the nonlinearities in the state equations depend only on the states that are fed back [50].

3.3   Non-overshooting Force Control of the μSEA

The *Introduction* section explains the idea behind the series elastic actuation. The main purpose of this design procedure is to control the force at the end effector of the μSEA. Among the force control strategies introduced in 3.1, the cascaded control approach of Wyeth, [32] is implemented.

In this cascaded structure, there is an inner position control loop and an outer force control loop. The inner loop of the control structure deals with imperfections (friction, sticktion, etc). In other words, inner control loop turns system into an effective position source, [32]. On top of this new structure, a force controller is implemented. The block diagram of the closed loop system can be seen in Figure 3.2.

In the simulation environment, two different reference inputs are supplied to the system in order to observe the response of the μSEA. The first input is a step input and the second one is a sinusoidal input. The magnitudes
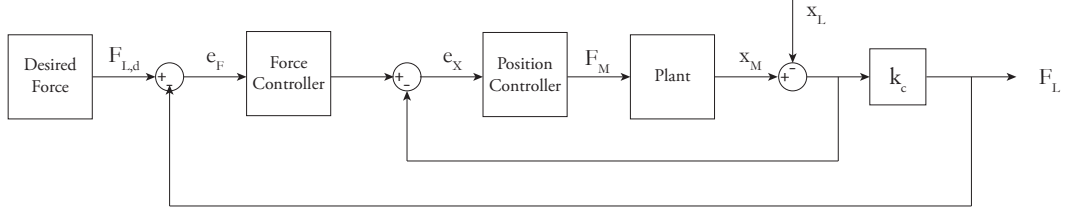
Figure 3.2: Block diagram of the closed loop system.

of these input signals are 1 N and the frequency of the sinusoidal signal is 0.015Hz.

For the step input, the response of the system is satisfactory. The response of the system and the displacement of the compliant element can be seen in Figures 3.3 and 3.4. Rise time of the μSEA for the step input is 0.021 seconds. The steady state error of the μSEA is 0.8%.

The table of parameters for this simulations can be found in Table 3.1.

Table 3.1: Table of parameters for force control simulation of μSEA.

Step Response	Simulation Time	0.1s
	Step Size	10^{-3}
	Solver	ODE4
Trajectory Tracking	Simulation Time	2s
	Step Size	10^{-3}
	Solver	ODE4
Position Controller	K_p	50
	K_i	1
Force Controller	K_p	2.5
	K_i	0.01
	K_d	0.1

For the sinusoidal input, the response of the system can be seen in Figure 3.5 and the displacement of the compliant element is in Figure 3.6. The response of the seems satisfactory, the root mean square error of the system wile tracing the sinudoidal trajectory is 0.2 Newton. As it is seen from Fig-

46
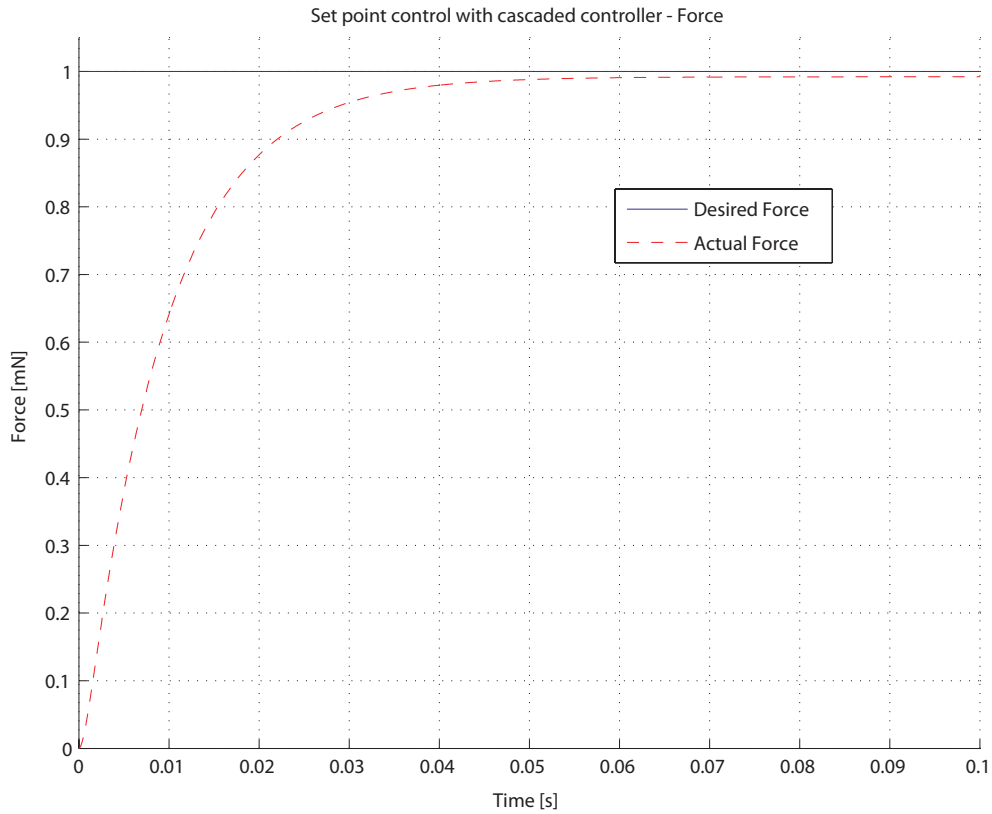
Figure 3.3: Set point force control of μSEA

ure 3.5, there is a little overshoot in the output force of μSEA and there is a phase lag between the input and output. This phase lag is due to the PI position controller.

Investigating Figures 3.4 and 3.6 reveals that the compliant element deflects about 8 μm. This information is especially valuable for choosing an appropriate actuator for the μSEA system.

3.3.1 Nonovershooting Force Controller Design

The cell manipulation example given in the first section of this chapter can also explain the need for a nonovershooting controller. In the same cell
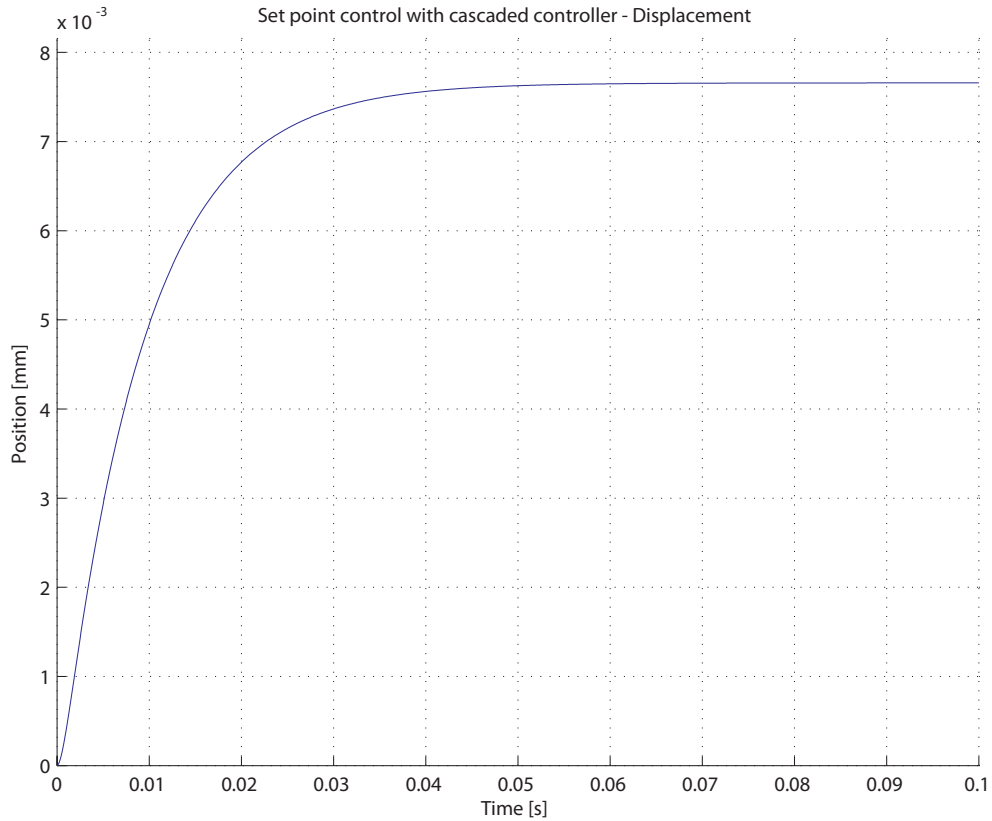
Figure 3.4: Displacement of the compliant coupling element of the μSEA in set point control

manipulation context, an overshoot that may occur during the operation will certainly degrade the reliance of the manipulator. Therefore, the controller used in force control should guarantee a nonovershooting response as the manipulator operates even in mediums that are unknown.

In the cascaded control structure, to achieve force control PID controllers are utilized in the previous section and it is observed that there may occure overshoot in the response. However, the motivation of the manipulation requires a non-overshooting force response for all the time. Therefore a controller is needed which satisfies a non-overshooting response characteris-

48
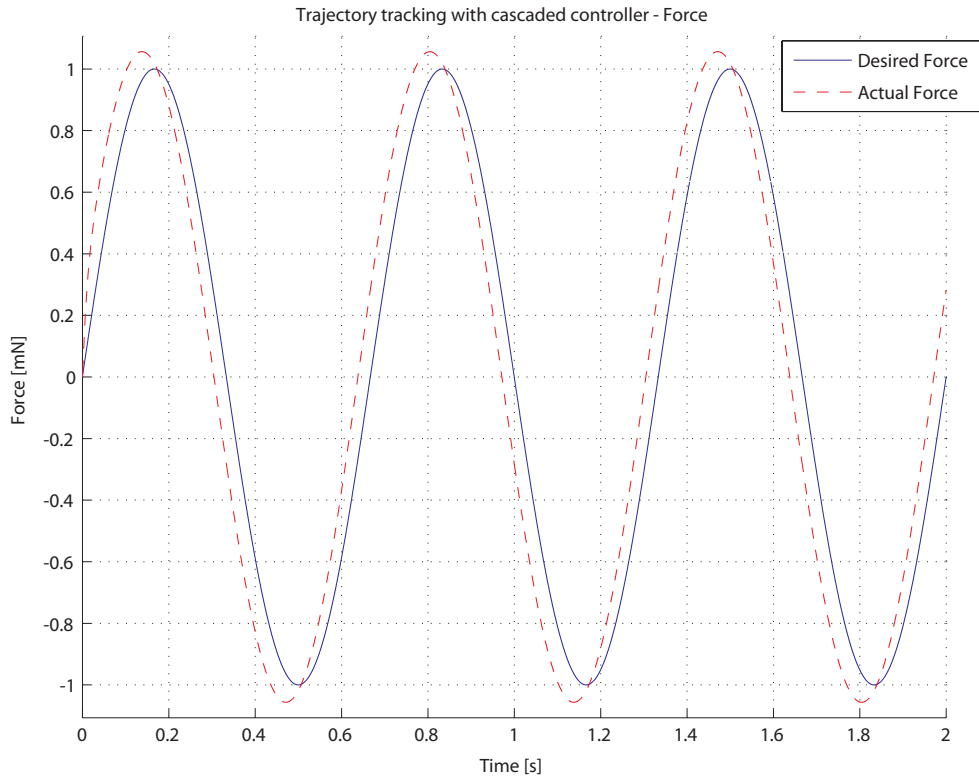
Figure 3.5: Sinusoidal force tracking of μSEA

tic. The non-overshooting response characteristic cannot be guaranteed with simple PD controller, because it may not satisfy an sign invariant impulse response.

The aim of this work is to establish a non-overshooting force controller. Most non-overshooting controllers proposed in the literature are designed for linear systems, and for nonlinear systems they rely on feedback linearization to obtain a linearized system so that the same controller design techniques can be used. However, as shown in [51], for a non-zero initial condition, the proposed linear non-overshooting controllers may fail; therefore, it is better to use a nonlinear design technique for a nonlinear system.

The non-overshooting controller designed in this paper, whose theory is

49
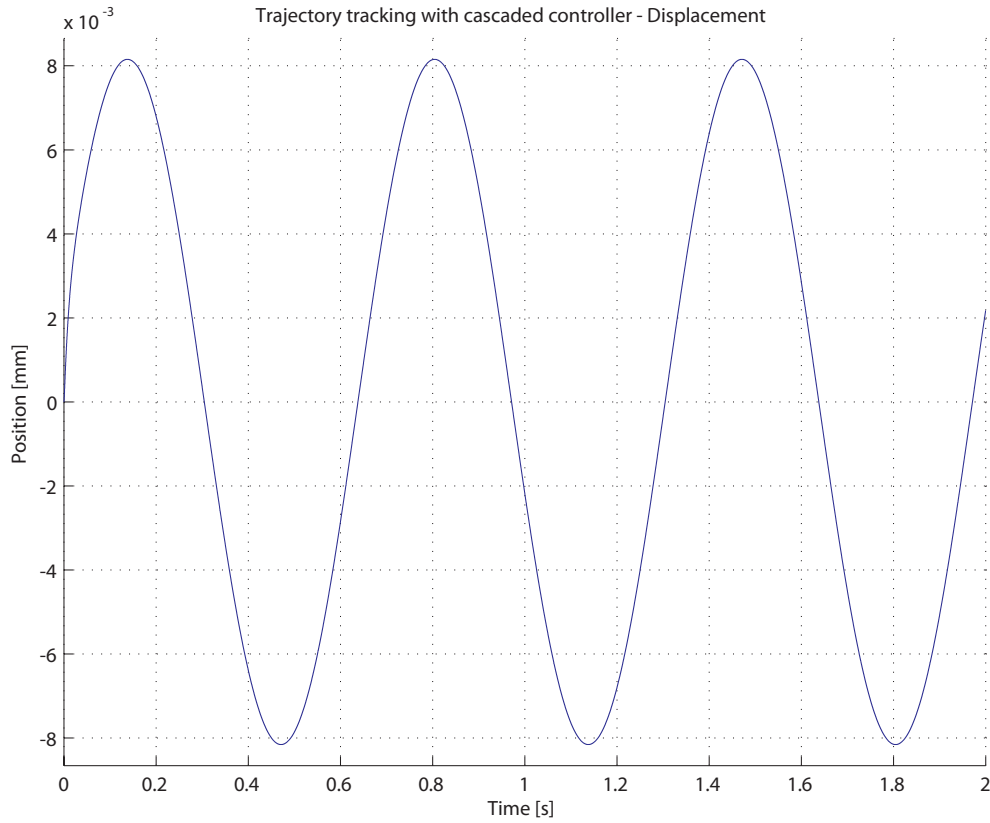
Figure 3.6: Displacement of the compliant coupling element of the μSEA in trajectory tracking

given in [51], is a backstepping controller. In backstepping controller, $(i+1)^{th}$ state element is used to stabilize the ith state equation and recursively this process is used to stabilize every state equation so that the overall system is stable. This technique maps the system into different coordinates where the new system is a diffeomorphism of the original system and a simple quadratic Lyapunov function is sufficient to ensure that the system is stable [52].

In order to achieve such a mapping, Krstic had proposed the following coordinate transformation for systems in the strict feedback form [51].

$$z_i = x_i - \alpha_{i-1}(x_1, \ldots, x_{i-1}, t) - r^{(i-1)}(t) \tag{26}$$

$$\alpha_i(x_1, \ldots, x_{i-1}, t) = -c_i z_i - \phi_i + \sum_{j=1}^{i-1} \frac{\partial \alpha_{i-1}}{x_j} [x_{j+1} + \phi_j] \tag{27}$$

where ϕ_i is the nonlinear terms in the ith state equation. The α_i in the transformation is referred as the nonlinear damping which improves the stability. The input to the system is given by,

$$u = \alpha_n \tag{28}$$

It has been shown in [51] that, the gains in the Equation 27 should be selected using the following rule,

$$\underline{c}_i = \frac{x_{i+1}(0) + \phi_i(x_i(0)) - \sum_{j=1}^{i-1} \left. \frac{\partial \alpha_{i-1}}{\partial x_j} \right|_{(x_j(0), 0)}}{(\alpha_{i-1}(x_i(0), 0) + r^{(i-1)} - x_i(0))} \tag{29}$$

$$c_i = max\{\underline{c}_i, 0\} \tag{30}$$

$$c_n > 0 \tag{31}$$

It should be noted that, the gain selection depends on the reference trajectory of the system; therefore, for every reference input, the gains have to be studied thoroughly so that the nonovershooting characteristic of the controller is preserved. The controller introduced in the above equations guarantees that the reference trajectory is traced without being exceeded, *i.e.* $y(t) \le r(t)$, $\forall t \ge 0$.

The design of the backstepping controller for the μSEA system will be

51

conducted using the state space model found in the previous section (Equation 25). The backstepping controller is implemented as a position controller. This position controller with an overdamped force controller can satisfy a nonovershooting force response. The block diagram of the closed loop system is presented in Figure 3.7.
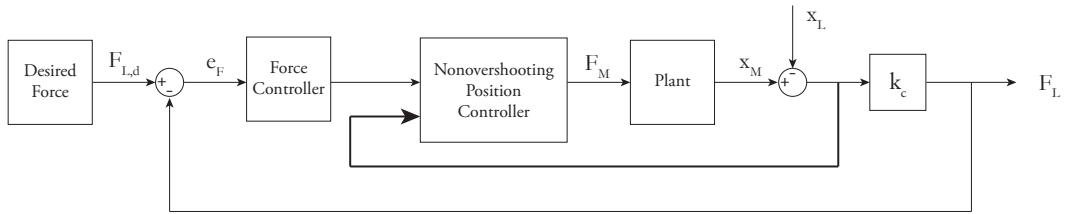

Figure 3.7: Block diagram of the closed loop system.

The simulation results of the μSEA with non-overshooting controller are presented in Figures 3.8, 3.9, 3.10 and 3.11. In the first simulation, a step function is given as the reference input. Referring to Figure 3.8, the rise time of the μSEA is 2.78 seconds. The steady stated error observed in the system is 1.58%. It is shown that, there is no overshoot in the response. In Figure 3.9, it is observed that the μSEA is deflecting $45\mu m$ for achiving a force of 3N.

In the second simulation a sinusoidal reference input is given to the system and the tracking performance is analyzed. The reference input to the system is in the form of $Asin(t) + B$. The RMS error occured during tacking is 0.0091N. It is observed from Figure 3.10 that the μSEA exhibits no overshoot. Figure 3.11 shows that the compliant mechanism deflects for $15\mu m$ while operating.

The simulation parameters of the non-overshooting force control is given in Table 3.2.
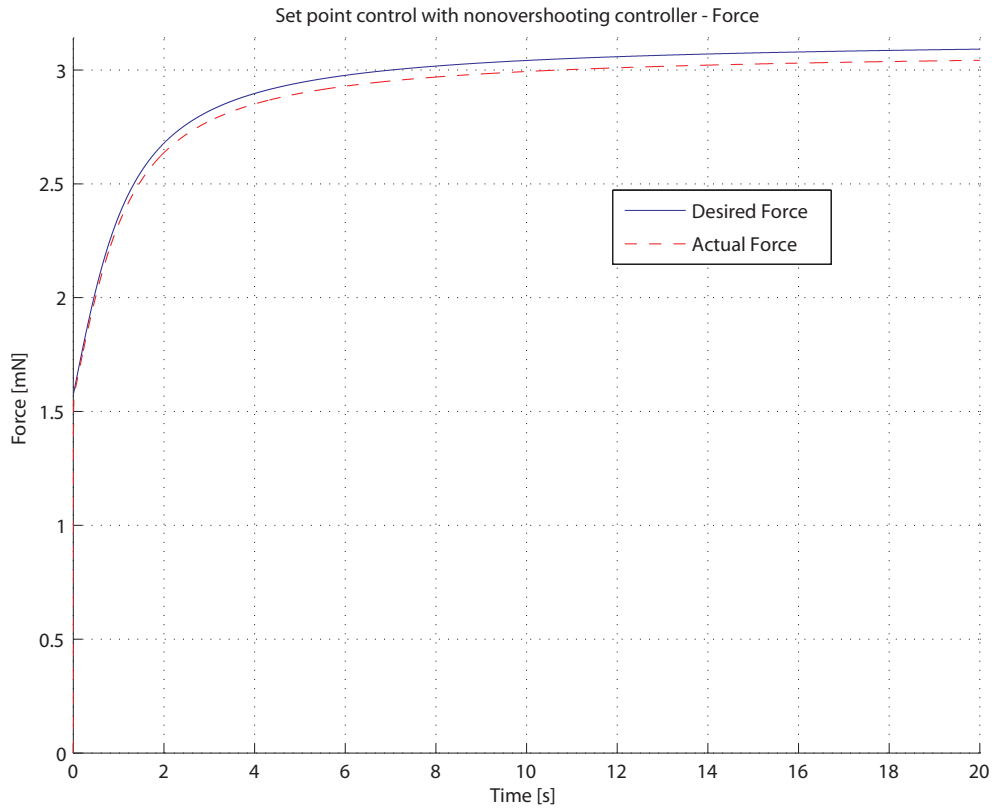
Figure 3.8: Set point force control of μSEA

3.4 μSEA in Teleoperation Scheme

The μSEA device can operate in autonomous mode where it can perform a predefined task while responding to the external world disturbances. This mode is especially preferable when the task has many repetitions with similar working conditions. However, the μSEA design can be run in another mode which is called the teleoperation mode where the micro-manipulator is driven by a human operator. This mode includes the involvement of a human, a high level logic, which can decide on the operation procedure as well as the task itself. The human operator may use the manipulator for exploring the micro world, such as analyzing the stiffness of the cell membrane or the operator
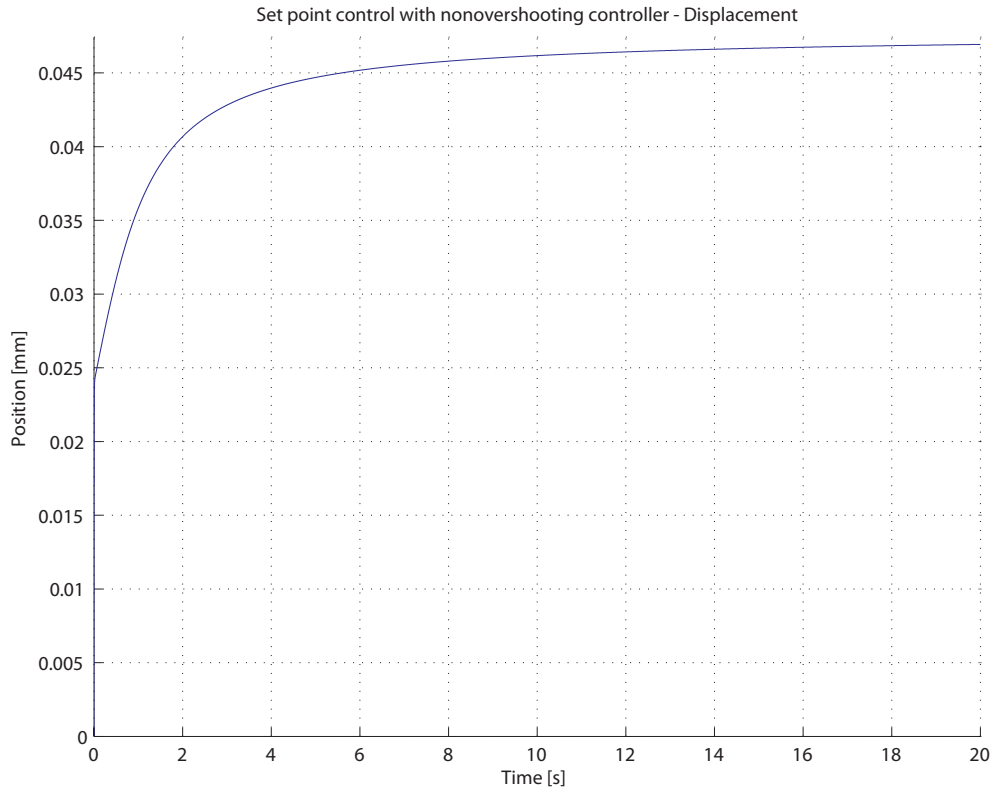
Figure 3.9: Displacement of the compliant coupling element of the μSEA in set point control

may complete a task like injecting drug into the cell. From this point of view, the involvement of a higher logic into the system may be beneficial; therefore, the μSEA device is embedded into a 3-channel teleoperation architecture.

The teleoperation is achieved using a pantograph mechanism as the master side robot and the μSEA as the slave side robot. The operator drives the pantograph mechanism to achieve micro manipulation through μSEA. However, it should be noted that, the master side robot, or the pantograph mechanisms, is a 2 degrees of freedom system whereas the slave side robot is a 1 degree of freedom μSEA. In order to have a correct mapping between the motions of master and slave robots, one degree of freedom of the pantograph
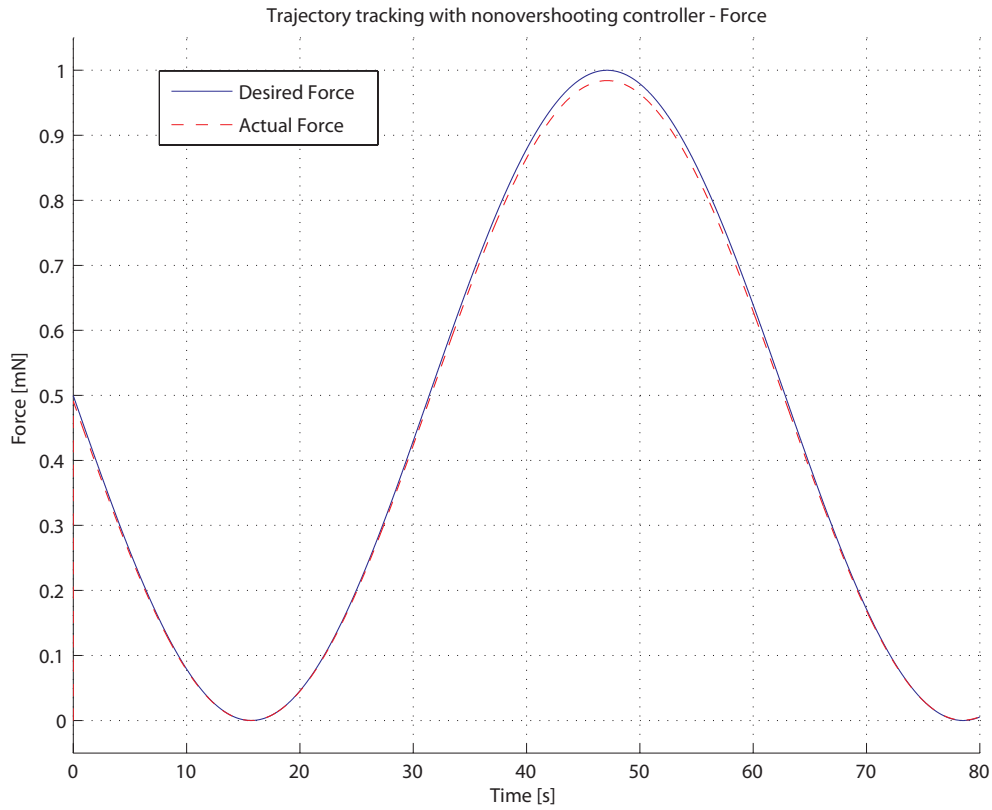
Figure 3.10: Sinusoidal force tracking of μSEA

mechanism is restricted using virtual walls.

There is a scale difference between the master and the slave sides of this teleoperation. In the master side, human operator is performing task using a pantograph mechanism. The motion range of the operator is in millimeter scale and the forces applied to the master device is in Newton scale. On the other hand, the slave side of the telemanipulator performs motion in micrometers and forces can be as low as miliNewtons. In the presence this scale difference the signal exchange between the master and slave is done by scaling the signal by a factor so that the magnitudes of the signals in master and slave sides are comparable. In the teleoperation architecture used in this
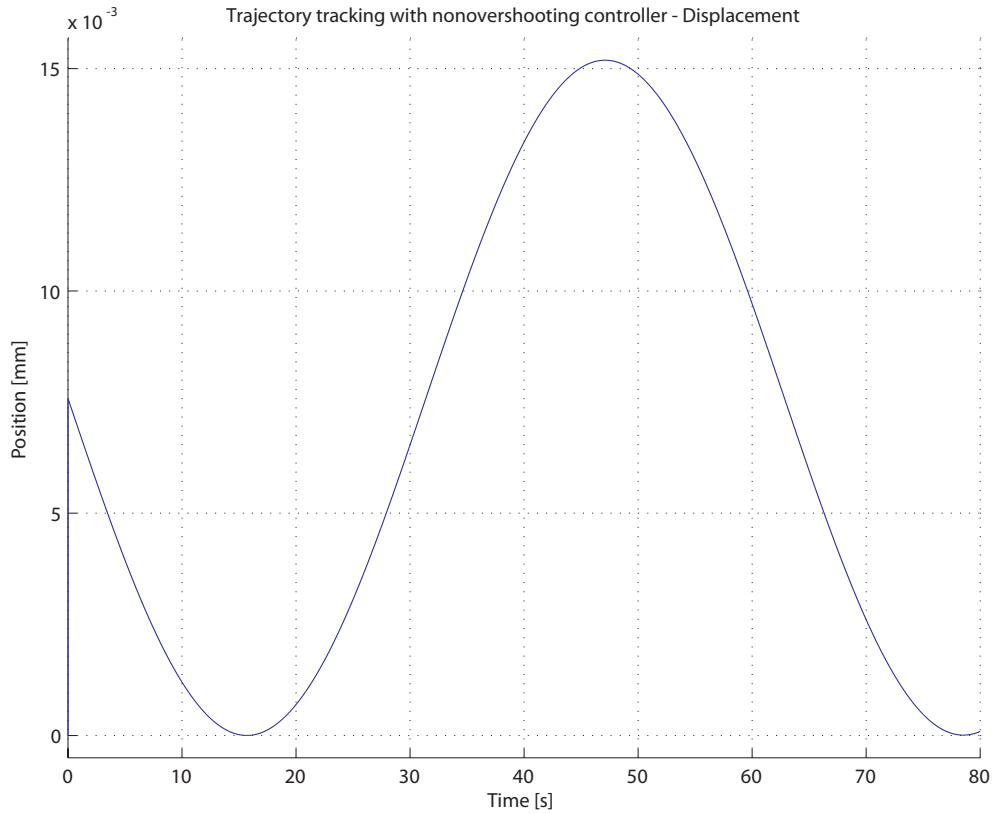
Figure 3.11: Displacement of the compliant coupling element of the μSEA in trajectory tracking

work, scaling factor is 10^3.

The teleoperation architecture used in this work is very similar to the 4-channel architecture introduced in [53] except one force channel, C_3, is not used in this teleoperation architecture. In 4-channel architecture, the force and position information of both the master and slave devices are passed to each other; however, in the teleoperaion structure used in this work uses slave position and force information with master's position information. The reason for omitting the force channel of master is that there is no force sensor mounted on the master device; therefore, it is not available to use.

Table 3.2: Table of parameters for non-overshooting force control simulation of μSEA.

Step Response	Simulation Time	20s
	Step Size	10^{-3}
	Solver	ODE4
Trajectory Tracking	Simulation Time	80s
	Step Size	10^{-3}
	Solver	ODE4
Position Controller	c_1	100
	c_2	10
Force Controller	K_p	0.001
	K_d	1

The structure of the 4-channel architecture can be seen in Figure 3.12.

In the 4-channel architecture, there is a master side of the teleoperator which is commanded by the human operator. On the other side of the teleoperator, there is the slave robot which interacts with the environment. There is a communication channel between the master and the slave and for 4-channel bilateral teleoperation, position and force informations of the master and the slave are send through these channels. The forces F_h^* and F_e^* are the forces applied by the human operator and the environment with respectively. These forces are independent of the teleoperation. Z_h and Z_e are the human and environment models.

The selection of the controllers of the teleoperation architecture, C_1, C_2, C_3, C_4, C_m, C_s, is done in such a way that the stability and the transperancy of the teleoperation is optimized, [53]. Preserving the stability is indispensable but not enough. In order to improve the quality of the teleoperation, *i.e.* eliminate the mushy feeling on the master side, transparency of the teleoperation should be maximized. In a perfect transparent teleoperator, the master and the slave manipulators behave exactly in the same motion and force,

however, transparency and stability are competing objectives. The optimum solution for best transparency and stability is choosing the the controllers of the system equivalent. For a complete discussion of transparency and stability of 4-channel architecture can be found in [53].

The stability of the of the teleoperated system can be decided using passivity analysis. Consider a two-port network shown in Figure 3.13. In this network model, v is the velocity of the manipulator and f is the force of the system. A network with an initial energy, E(0), is passive if and only if, [54],

$$\int_0^t (f_1(\tau)v_1(\tau) + f_2(\tau)v_2(\tau))d\tau + E(0) \geq 0, \quad t \geq 0 \tag{32}$$

Passivity can be read as: for a system with an initial energy, if the system is not generating energy, then it can be said that the system is passive. Assuming that the system is zero state observable, passivity implies that the system is stable. It should be noted that, although a passive system is stable, it is not always possible to says that a stable system is passive. Hence, it can be deduced that, passivity is a conservative way of indicating the systems stability.

For the bilateral teleoperation architecture, the passivity of the system is analyzed for its sub components. The human operator is assumed to be passive. The master and slave robots are passive devices (since all unactuated physical systems are passive). The controller used in the master side, which is a PD, is a passive controller. On the slave side, the non-overshooting controller, which is a backstepping controller, is also passive [50]. Therefore, only the passivity of the communication channel is questionable. In the

presence of time delay, passivity of the communication channel cannot be guaranteed. However, the implementation of micro-telemanipulation device will be made on the same computer, *i.e.* there will not be a time delay between the master and slave devices. Hence the communication channel without time delay is passive. Since all components of the teleoperation architecture is passive the overall system is passive, *i.e.* the overall system is stable.

As it is explained, the teleoperator with the 4-channel architecture is stable. On the other hand, related with the stability issues, there is one more analysis that should be conducted on the micro-teleoperation system. The master side of this teleoperator is a rigid pantograph mechanism and the slave side is a soft micro-manipulator. Unlike most teleoperation examples of the literature which include rigid robot for both master and slave, this telemanipulation system uses a hard-soft teleoperation structure which is analyzed in [55, 56].

Christiansson *et al.* analyzed theoretically and experimentally that the stiffness of the slave operator can improve the stability of the teleoperation especially when the environment is stiff. Although the stability of the contact with the stiff environment can be improve with passive compliance added to the slave operator, the feel of the environment at the master side will be mushy because of the filtering effect of the passive compliance. In [55], it had been showed that, as the stiffness of the slave robot decreases the stability of the teleoperation during contract with the remote environment (and in the presence of time-delay) is improved. Moreover, in [56], it is experimentally verified that, adding a passive compliance to the slave manipulator improves the stability of the teleoperation.

The micro-telemanipulation system developed in this thesis adopts the hard-soft teleoperation principle of Christiansson. The slave manipulator, μSEA, is a soft robot which inherently has a passive compliance. Not surprisingly, while listing the advantages of SEA, it has been said that compliance in the SEA is beneficial if there is a hard contact (impact) between the SEA and the object. Here, in the teleoperation device, this advantage of the SEAs is utilized in hard-soft teleoperation scheme.

The simulations of the hard-soft teleoperation in 3-channel architecture is held in Simulink environment. The results can be seen in Figures 3.15 and 3.14. In order to compare the position and force values of master and slave devices, the signals of slave has been scaled by 10^3 in the plots. As it can bee seen in the figures, the force and position tracking of the teleoperation is very satisfactory. On the other hand, the slave device do not overshoot the master device force or position. In force tracking, the RMS error is 2mN and in position tracking, the RMS error is $0.3\mu m$.

The parameters used in the teleoperation simulation can be found in Table 3.3.

Table 3.3: Table of parameters for teleoperation of μSEA.

|			
Simulation	Simulation Time		50s
	Step Size		10^{-3}
	Solver		ODE4
Communication Channel	C_1		1
	C_2	K_m	1000
		b_m	1000
	C_4		1
Master Side Controller	K_p		10
	K_d		1
Slave Side Controller	c_1		10000
	c_2		100
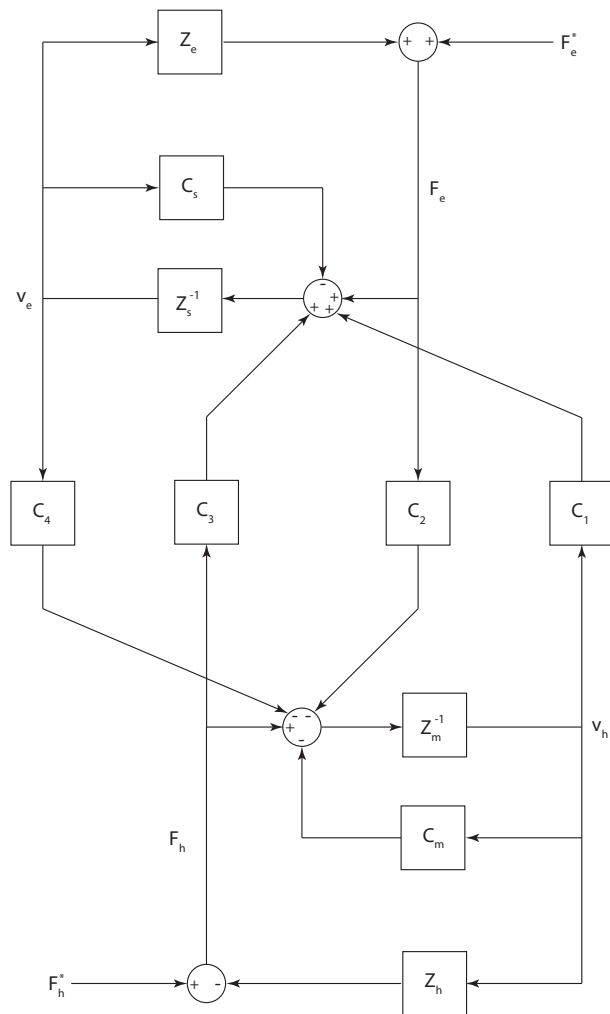
Figure 3.12: 3-channel teleoperation architecture
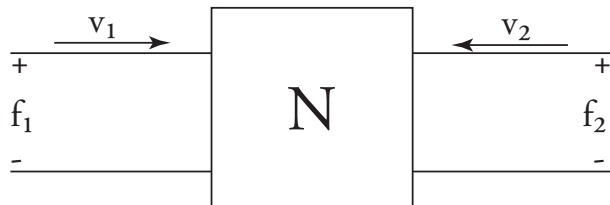

Figure 3.13: A two-port network
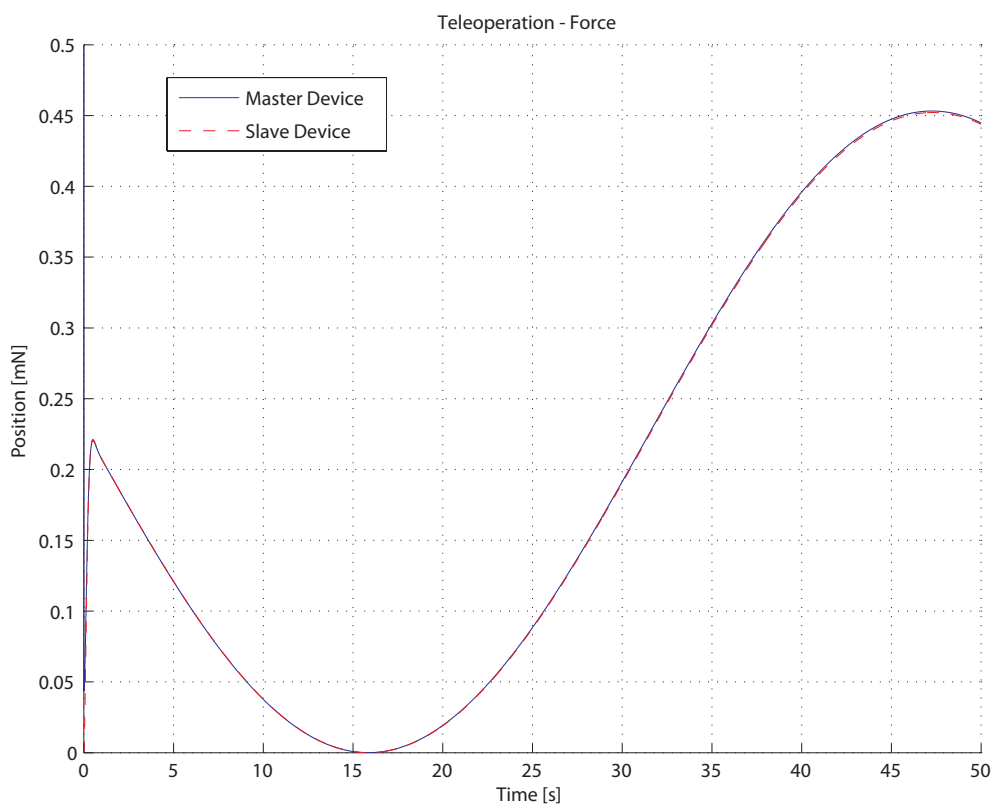
Figure 3.14: Force tracking teleoperation results for master (slider-cranck) slave (μSEA) system. The force information of slave is scaled by 10^3
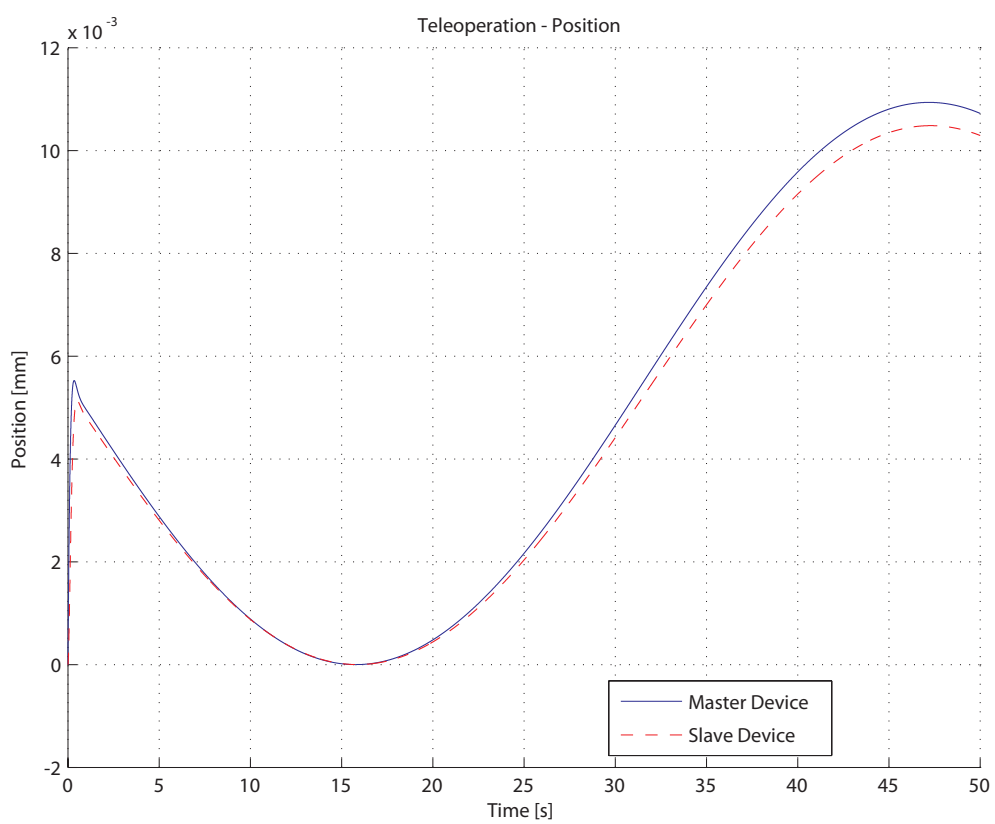
Figure 3.15: Position tracking teleoperation results for master (slider-crank) slave (μSEA) system. The position information of slave is scaled by 10^3

Chapter IV

4 Implementation and Verification

This chapter explains the testbed used in the experiments and presents the experimental verification of the developed mechanical system with its controllers.

4.1 Experimental Setup

In order to validate the designed μSEA based teleoperator two testbeds are designed and built. The first testbed is used to validate the performance and the non-overshooting force control ability of the μSEA and the second one is used to test the μSEA in a teleoperation architecture.

The first testbed is constructed to test the force control performance of the μSEA. The components of the testbed are: μSEA and a force sensor. It should be noted that the force sensor mounted on the testbed is not used on the feedback line, instead, force sensor is just used to measure the force that is exerted by the μSEA. The testbed can be seen in Figure 4.1 and Figure 4.2. The μSEA part of the testbed is explained in Section 2.7.

The second test setup is build for teleoperation experiments. In this setup, the μSEA testbed used as the slave device of the teleoperator and a pantograph mechanism is implemented as the master device. It should be noted that, the slave device has 1 degree of freedom whereas the master
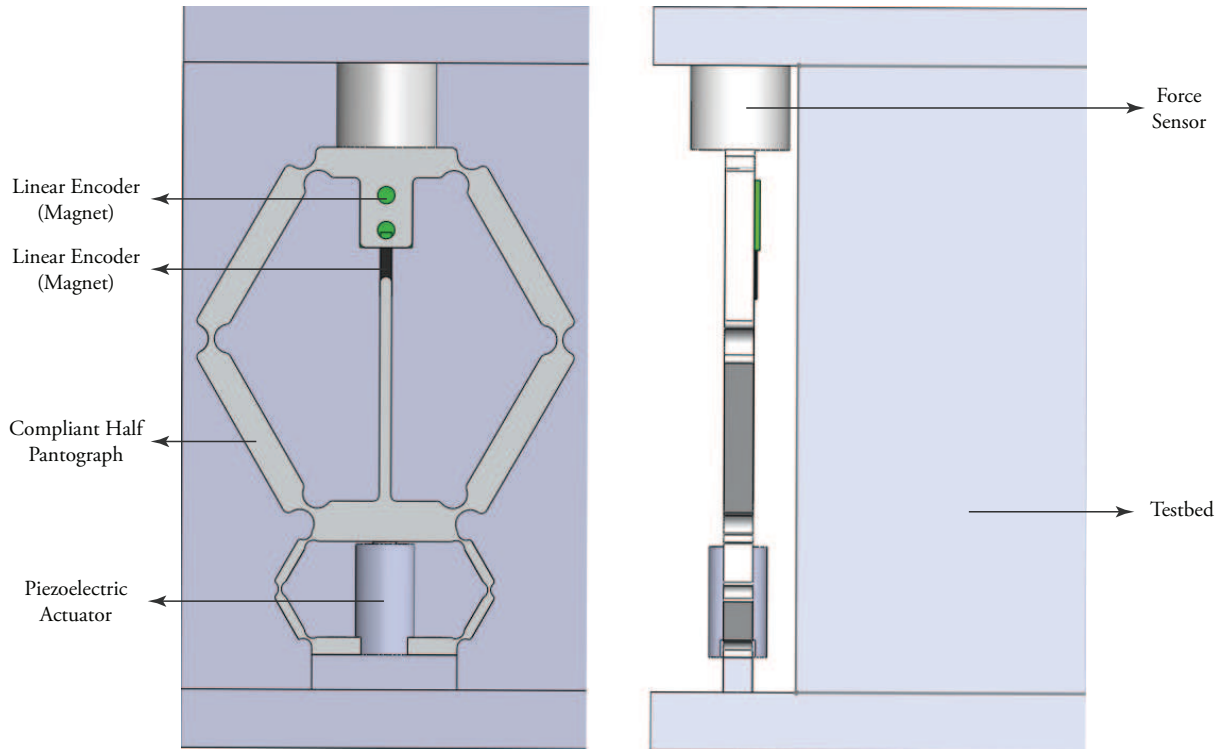
Figure 4.1: μSEA and the testbed used in the experiments – CAD drawing

has 2 degrees of freedom. In order to make the devices compatible, the master robot, *i.e.* the pantograph mechanism, is restricted to move in a single direction by using virtual walls. The master and the slave robots are commanded using the same control card; therefore there is no significant time delay in the teleoperation.

The real-time control of the both experiments are conducted using the Quaser Q8 Real-Time Control Card. This card has 8 channels with 12-bit D/A voltage outputs and 8 quadrature encoder input. It is compatible with most analog and digital sensors and supports Matlab RTW. As the real-time operating system, Windows Xp with RTX real-time extension is used. This extension adds hard real-time features by by-passing the Windows Xp's
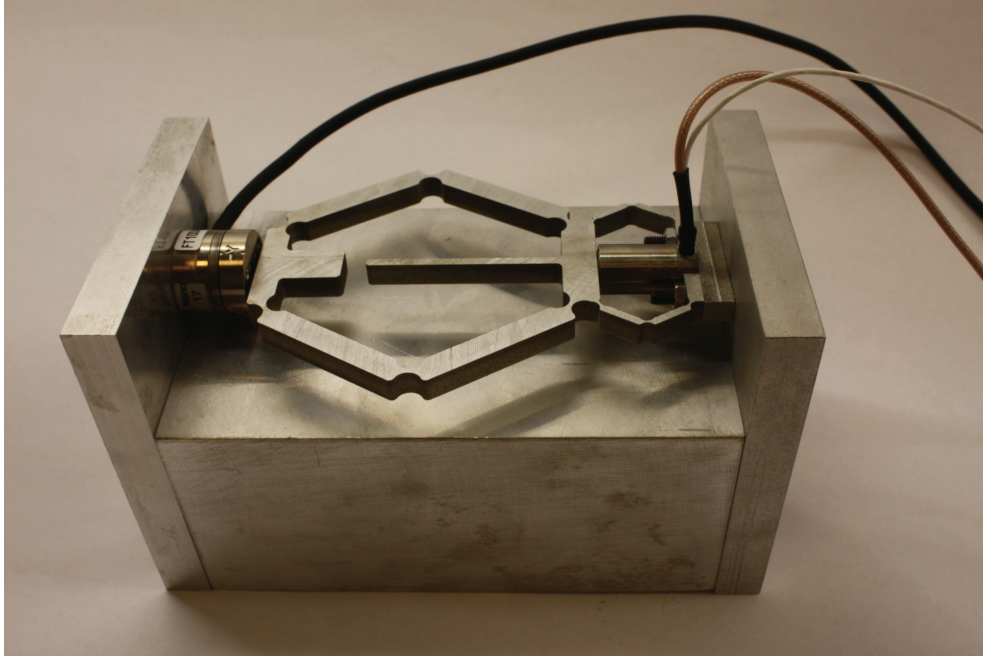
Figure 4.2: μSEA and the testbed used in the experiments

scheduler. Wincon control software is used to communicate between the RTX and the Q8. Wincon is a simple interface designed for control purposes by Quanser and it is compatible with Matlab/Simulink.

4.2 Experimental Verification

The μSEA device and the testbed are ready for the experiments. The verification of the proposed design and controllers will be verified in the immediate future.

Chapter V

5   Conclusion and Future Work

This thesis had introduced a (μSEA) which is used in manipulation of micro objects. The μSEA is introduced in two sections: design and control. Since an SEA is a dazzling mechatronic device, design and control should not be seperated from each other. Thereforce in this thesis optimal design with high performace controllers are developed for the μSEA.

In the design of the μSEA, optimality and the reliability of the design is considered to have a high quality device. The performance of the μSEA is measured using manipulability and stiffness metrics. The manipulability of the system along it actuation direction is increased to have higher dexterous workspace, also stiffness of the device is decreased along this direction in order to have a better force accuracy. Along the direction perpendicular to the actuation direction, the manipulaility is decreased and stiffness is increased so that the disturbance characteristic of the system is improved. This optimal dimensioning problem, which has multiple criteria, is solved using the method called Normal Boundary Intersection method (NBI). Simultaneously, while searching for the optimal design variables that increase the performance, the reliability of the system is also considered. The robustness criteria and performance metrics are optimized at the same to have a solution set that is both satisfy the performance and reliability considerations. A configuration

from the robust Pareto set is chosen as the final configuration.

The robust optimal configuration is tested for its force control performance. The force control is conducted using two controllers: a cascaded force controller and a nonovershooting force controller. The cascaded force controller has an inner position controller and an outer position controller. The inner controller loop turns the system into a pure position source and on top of this new system a force controller is implemented to achive high performance force control. Although this controller has satisfactory results, the force response of the system is not guaranteed to be nonovershooting. If the application demands a nonovershooting force response, like a cell indentation procedure, then a overshoot-free controller should be implemented. The position controller of the previous controller replaced with a nonovershooting position controller, therefore the output force of the system is guaranteed to the below the reference input. Finally, the μSEA is embedded into a 3-channel scaled teleoperation architechture so that a human operator can perform manipulation in a micro level.

The future work of this project is to implement the force control algorithms and test the force control quality of the system. Once the SEA concept for microsystems is shown to be efficient, a new system with a much lower stiffness rates will be design for a cell indentation setup which will be an automated testbed for controlling the stiffness of cell membranes.

References

[1] Michel Wautelet. Scaling laws in the macro-, micro- and nanoworlds. *European Journal of Physics*, 22:601 – 611, 2001.

[2] G. Binnig and C. F. Quate. Atomic Force Microscope. *Physical Review Letters*, 56(9):930 – 934, 1986.

[3] Arthur Ashkin. Acceleration and Trapping of Particles by Radiation Pressure. *Physical Review Letters*, 24(4):156 – 159, 1970.

[4] Arthur Ashkin. Optical Trapping and Manipulation of Neutral Particles Using Lasers. *Proceedings of National Academy of Science USA*, 94:4853 – 4860, 1997.

[5] M. Goldfarb and N. Celanovic. A Flexure-based Gripper for Small-scale Manipulation. *Robotica*, 17:181 – 187, 1999.

[6] R. M. Voyles and S. Hulst. Micro/macro force-servoed gripper for precision photonics assembly and analysis. *Robotica*, 23:401 – 408, 2005.

[7] K. Han, S. H. Lee, W. Moon, and J-S. Park. Fabrication of the microgripper with a force sensor for manipulating a cell. In *SICE-ICASE International Joint Conference*, October 2006.

[8] Young bong Bang, Kyung min Lee, J. Kook, Wonseok Lee, and In su Kim. Micro parts assembly system with micro gripper and rcc unit. *Robotics, IEEE Transactions on*, 21(3):465 – 470, june 2005.

[9] S. Stoyanov, C. Bailey, R. Leach, B. Hughes, A. Wilson, W. O'Neill, R.A. Dorey, C. Shaw, D. Underhill, and H.J. Almond. Modelling and

prototyping the conceptual design of 3d cmm micro-probe. In *Electronics System-Integration Technology Conference, 2008. ESTC 2008. 2nd*, pages 193 –198, 1-4 2008.

[10] Xi Wenming and Zhong Hui. Bio-manipulation probe integration with micro-force sensor. In *Nano/Micro Engineered and Molecular Systems, 2008. NEMS 2008. 3rd IEEE International Conference on*, pages 393 –396, 6-9 2008.

[11] Jung Yup Kim, Hak Joo Lee, Hyun Ju Choi, S.J. Lee, and Sung Wook Moon. Design, fabrication and mechancial characterization of vertical micro contact probe. In *Sensors, 2006. 5th IEEE Conference on*, pages 1155 –1158, 22-25 2006.

[12] Guangyong Li, Ning Xi, Mengmeng Yu, F. Salem, D.H. Wang, and Jianping Li. Manipulation of living cells by atomic force microscopy. In *Advanced Intelligent Mechatronics, 2003. AIM 2003. Proceedings. 2003 IEEE/ASME International Conference on*, volume 2, pages 862 – 867, 20-24 2003.

[13] V. Parpura, P. G. Haydon, D. S. Sakaguchi, and E. Henderson. Atomic force microscopy and manipulation of living glial cells. *Journal of Vacuum Science Technology A: Vacuum, Surfaces, and Films*, 11(4):773 –775, july 1993.

[14] D. G. Grier. A Revolution in Optical Manipulation. *Nature*, 424:810 – 816, August 2003.

[15] I. Bukusoglu, C. Basdogan, A. Kiraz, and A. Kurt. Haptic manipulation of microspheres using optical tweezers. In *Haptic Interfaces for Virtual*

Environment and Teleoperator Systems, 2006 14th Symposium on, pages 361 – 365, 25-26 2006.

[16] Yanhua Wu, Youhua Tan, Dong Sun, and Wenhao Huang. Force analysis and path planning of the trapped cell in robotic manipulation with optical tweezers. In *Robotics and Automation (ICRA), 2010 IEEE International Conference on*, pages 4119 –4124, 3-7 2010.

[17] R. Volpe and P. Khosla. A theoretical and experimental investigation of explicit force control strategies for manipulators. *Automatic Control, IEEE Transactions on*, 38(11):1634 –1650, nov 1993.

[18] N. Hogan. Impedance Control: An Approach to Manipulation: Part I—Theory. *Journal of Dynamic Systems, Measurement and Control*, 107(1), 1985.

[19] G. Zeng and A. Hemami. An overview of robot force control. *Robotica*, 15:473 – 482, 1997.

[20] S. Eppinger and W. Seering. Understanding bandwidth limitations in robot force control. In *Robotics and Automation. Proceedings. 1987 IEEE International Conference on*, volume 4, pages 904 – 909, mar 1987.

[21] J. W. Sensinger and R. F. ff. Weir. Improvements to series elastic actuators. In *IEEE/ASME International Conference on Mechatronic and Embedded Systems and Applications*, 2006.

[22] J. W. Sensinger and R. F. {ff.} Weir. Unconstrained impedance control using a compact series elastic actuator. In *IEEE/ASME International*

Conference on Mechatronic and Embedded Systems and Applications, 2006.

[23] G. A. Pratt and M. M. Williamson. Series elastic actuators. In *IEEE International Conference on Intelligent Robots and Systems*, 1995.

[24] J. E. Pratt, B. T. Krupp, C. J. Morse, and S. H. Collins. The RoboKnee: an exoskeleton for enhancing strength and endurance during walking. In *IEEE International Conference on Robotics & Automation*, 2004.

[25] J. F. Veneman, R. Ekkelenkamp, R. Kruidhof, F. C. T. van der Helm, and H. van der Kooij. A Series Elastic- and Bowden-Cable-Based Actuation System for Use as Torque Actuator in Exoskeleton-Type Robots. *The International Journal of Robotics Research*, 25(3):261–281, 2006.

[26] H. Herr and A. Wilkenfeld. User-adaptive Control of a Magnetorheological Prosthetic Knee. *Industrial Robot: An International Journal*, 30(1):42–55, 2003.

[27] G. A. Pratt. Low Impedance Walking Robots. *Integrative and Comparative Biology*, 42(1):174–181, 2002.

[28] D. W. Robinson, J. E. Pratt, D. J. Paluska, and G. A. Pratt. Series elastic actuator development for a biomimetic walking robot. In *IEEE/ASME International Conference on Advance Intelligent Mechatronics*, 1999.

[29] D. Paluska and H. Herr. The Effect of Series Elasticity on Actuator Power and Work Output: Implications for Robotic and Prosthetic Joint Design. *Robotics and Autonomous Systems*, 54:667–673, 2006.

[30] J. W. Sensinger and R. F. ff. Weir. Design and analysis of a non-backdrivable series elastic actuator. In *IEEE 9th International Conference on Rehabilitation Robotics*, 2005.

[31] J. S. Sulzer, M. A. Peshkin, and J. L. Patton. Pulling your strings. *IEEE Robotics & Automation Magazine*, 15(3):70–78, 2008.

[32] G. Wyeth. Demonstrating the safety and performance of a velocity sourced series elastic actuator. In *IEEE International Conference on Robotics and Automation*, 2008.

[33] H. Vallery, J. Veneman, E. van Asseldonk, R. Ekkelenkamp, M. Buss, and H. van Der Kooij. Compliant actuation of rehabilitation robots. *IEEE Robotics & Automation Magazine*, 15(3):60–69, 2008.

[34] J. P. Merlet. *Parallel Mechanisms*. Springer-Verlag, 2006.

[35] A. J. Nielson and L. L. Howell. An Inverstigation of Compliant Micro Half Pantographs Using the Pseudorigid Body Model. *Mechanics Based Design of Structures and Machines*, 29:317 – 330, 2001.

[36] L. L. Howell. *Compliant Mechanisms*. John Wiley and Sons., 2001.

[37] B. H. Kang, J. T.-Y. Wen, N. G. Dagalakis, and J. J. Gorman. Analysis and Design of Parallel Mechanisms with Flexure Joints. *IEEE Transactions on Robotics*, 21(6):1179–1185, 2005.

[38] T. Yoshikawa. Manipulability of Robotic Mechanisms. *International Journal of Robotics Research*, 4:3–9, 1985.

[39] O. Tokatli and V. Patoglu. Multi-cirteria design optimization of a compliant micro half-pantograph. In *ECCOMAS Thematic Conferences on Multibody Dynamics*, 2009.

[40] R. Unal, G. Kiziltas, and V. Patoglu. A multi-criteria design optimization framework for haptic interfaces. In *IEEE International Symposium on Haptic Interfaces for Virtual Environments and Teleoperator Systems*, 2008.

[41] R. Unal and V. Patoglu. Optimal dimensional synthesis of a dual purpose haptic exoskeleton. In *Springer in the Lecture Notes in Computer Science, EuroHaptics08*, 2008.

[42] I. Das and J. E. Dennis. Normal-boundary Intersection: A new Method for Generating the Pareto Surface in the Nonlinear Multi-criteria Optimization Problems. *SIAM Journal on Optimization*, 8(3):631–665, 1996.

[43] E. Rigoni and S. Poles. NBI and MOGA-II, two tomplementary algorithms for multi-objective optimizations. In *Practical Approaches to Multi-Objective Optimizations*, 2005.

[44] S. Gunawan and S. Azarm. Non-gradient based parameter sensitivity estimation for single objective robust design optimization. *Journal of Mechanical Design*, 126:395 – 402, 2004.

[45] R. Unal, G. Kiziltas, and V. Patoglu. A multi-criteria design optimization framework for haptic interfaces. In *IEEE International Symposium on Haptic Interfaces for Virtual Environments and Teleoperator Systems*, 2008.

[46] S. Gunawan and S. Azarm. Multi-objective robust optimization using a sensitivity region concept. *Strctural Multidisciplinary Optimization*, 29:50 – 60, 2005.

[47] C. M. Fonseca and P. J. Fleming. Genetic algorithms for multiobjective optimization: Formulation, discussion and generalization. *Multiobjective Evolutionary Algorithms: Empirical Genetic Algorithms*, pages 416–423, 1993.

[48] J. W. Sensinger and R. F. ff. Weir. Unconstraint Impedance Control Using a Compact Series Elastic Actuator. In *IEEE/ASME International Conference on Mechatronic and Embedded Systems and Applications*, 2006.

[49] G. A. Pratt, P. Williamson, C. Bolton, and A. Hofman. Late Motor Processing in Low-Impedance Robots: Impedance Control of Series Elastic Actuators. In *American Control Conference*, 2004.

[50] Miroslav Krstic and Ioannis Kanellakopoulos and Petar V Kokotovic. *Nonlinear and Adaptive Control Design*. Wiley-Interscience, 1995.

[51] Miroslav Krstic and Matt Bement. Nonovershooting control of strict-feedback nonlinear systems. *IEEE Transactions on Automatic Control*, 51(12):1938 – 1943, 2006.

[52] Shankar Sastry. *Nonlinear Systems: analysis, stability and control*. Springer-Verlag, 1999.

[53] Dale A. Lawrence. Stability and Transparency in Bilateral Teleoperation. *IEEE Transactions on Robotics and Automation*, 9(5):624 – 635, October 1993.

[54] Jee-Hwan Ryu, Dong-Soo Kwon, and B. Hannaford. Stable teleoperation with time-domain passivity control. *Robotics and Automation, IEEE Transactions on*, 20(2):365 – 373, april 2004.

[55] G. A. V. Christiansson, M. Mulder, and F. C. T. van der Helm. Slave Device Stiffness and Teleoperator Stability. In *Eurohaptics Conference*, 2006.

[56] Göran Christiansson. An Experimental Study of Haptic Feedback in a Teleoperated Assembly Task. *Journal of Computing and Information Science in Engineering*, 8, December 2008.